

Bulletin of Earthquake Engineering

A ground motion model for volcanic areas in Italy

--Manuscript Draft--

Manuscript Number:	BEEE-D-19-00231R1
Full Title:	A ground motion model for volcanic areas in Italy
Article Type:	Original Research
Keywords:	Ground motion model; Volcano earthquakes; Italy; Epistemic uncertainty
Corresponding Author:	Giovanni Lanzano, Ph.D. Istituto Nazionale di Geofisica e Vulcanologia Milano, MI ITALY
Corresponding Author Secondary Information:	
Corresponding Author's Institution:	Istituto Nazionale di Geofisica e Vulcanologia
Corresponding Author's Secondary Institution:	
First Author:	Giovanni Lanzano, Ph.D.
First Author Secondary Information:	
Order of Authors:	Giovanni Lanzano, Ph.D. Lucia Luzi
Order of Authors Secondary Information:	
Funding Information:	
Abstract:	In Italy, earthquakes caused by volcanoes are of primary importance in the evaluation of seismic hazard, since several volcanoes seriously endanger densely populated areas (e.g. Catania and surroundings, Campi Flegrei, Vesuvius). On the other hand, there are very few models for the prediction of ground motion induced by volcanic events, mostly because observations are scarce and volcanic earthquakes less frequent than crustal events. Following the recent earthquakes in the Etna area (mainshock 26/12/2018 Mw = 4.9) and in the island of Ischia (mainshock 21/08/2017 Mw = 3.9), it was possible to increase the number of recordings for volcanic areas in Italy and, in particular, close to the epicentre. The data available after the recent events revealed the limitations of previous models and especially their inadequacy to predict the ground motion observed in the near source, that can be unexpectedly high. We calibrate a new empirical model to predict the amplitudes of several intensity measures for volcanic areas in Italy. The most relevant aspect in the proposed model is the different attenuation with the distance between shallow and deep events, with discerning focal depth fixed at 5km. The equations are valid for the geometric mean of horizontal components of PGA, PGV and acceleration response spectra ordinates at 5% damping (in period range $T = 0.025 - 5s$). The range of validity in magnitude is 3.5 - 4.9 and the hypocentral distance range is 1 - 200 km.
Suggested Reviewers:	Gail Atkinson Full Professor, University of Western Canada gatkings6@uwo.ca She is an expert in ground motion models and calibrated a model for Hawaii volcano earthquakes in 2010 Graeme Weatherill GFZ-Potsdam graeme.weatherill@gfz-potsdam.de He is the responsible of the update of the ground motion logic tree for European hazard model in the SERA EU project. Roberto Paolucci Full professor, Technical University of Milano

	roberto.paolucci@polimi.it As member of the Italian Risk Committee (Commissione Grandi Rischi) he is interested in this research
Response to Reviewers:	The reply to the reviewer's is in the attached document

[Click here to view linked References](#)

A ground motion model for volcanic areas in Italy

Giovanni Lanzano¹ and Lucia Luzi²

1. *Istituto Nazionale di Geofisica e Vulcanologia, Via Corti 12, Milan, Italy; email: giovanni.lanzano@ingv.it; ORCID: <http://orcid.org/0000-0001-7947-4281>; phone: +3923699260 (corresponding)*
2. *Istituto Nazionale di Geofisica e Vulcanologia, Via Corti 12, Milan, Italy; email: lucia.luzi@ingv.it; ORCID: <http://orcid.org/0000-0003-4312-580X>; phone: +3923699285*

Abstract:

In Italy, earthquakes caused by volcanoes are of primary importance in the evaluation of seismic hazard, since several volcanoes seriously endanger densely populated areas (e.g. Catania and surroundings, Campi Flegrei, Vesuvius). On the other hand, there are very few models for the prediction of ground motion induced by volcanic events, mostly because observations are scarce and volcanic earthquakes less frequent than crustal events. Following the recent earthquakes in the Etna area (mainshock 26/12/2018 $M_w = 4.9$) and in the island of Ischia (mainshock 21/08/2017 $M_w = 3.9$), it was possible to increase the number of recordings for volcanic areas in Italy and, in particular, close to the epicentre. The data available after the recent events revealed the limitations of previous models and especially their inadequacy to predict the ground motion observed in the near source, that can be unexpectedly high.

We calibrate a new empirical model to predict the amplitudes of several intensity measures for volcanic areas in Italy. The most relevant aspect in the proposed model is the different attenuation with the distance between shallow and deep events, with discerning focal depth fixed at 5km.

The equations are valid for the geometric mean of horizontal components of PGA, PGV and acceleration response spectra ordinates at 5% damping (in period range $T = 0.025 - 5s$). The range of validity in magnitude is 3.5 - 4.9 and the hypocentral distance range is 1 - 200 km.

Keywords: Ground motion model; Volcano earthquakes; Italy; epistemic uncertainty

Submitted to: Bulletin of Earthquake Engineering

1. Introduction

Ground Motion Models (GMMs) are used to predict peak parameters and spectral amplitudes as a function of some explanatory variables such as magnitude, distance and proxies of site effects, and are considered as one of the key ingredients in the seismic hazard assessment. Empirical GMMs are commonly calibrated using strong motion recordings of the region of interest or other regions, characterized by a similar tectonic environment. As a matter of fact, GMMs for shallow active crustal regions cannot be used in other seismotectonic regions, such as subduction or volcanic zones, since the ground motion is characterized by different features. In particular, volcanic earthquakes occur as magma and volcanic gases rise to the surface from depth, which involves significant stress changes in the crust as the material migrates upward (<https://volcanoes.usgs.gov/vhp/earthquakes.html>). Two main types of earthquakes induced by volcanic activities are recognized: i) Long-period (LP) earthquakes, caused by cracks resonating as magma and gases move toward the surface; ii) Volcano-tectonic (VT) earthquakes that represent a brittle failure of rock, the same process that occurs along purely "tectonic" faults.

Looking at the waveforms of LP earthquakes, Pitt and Hill (1994) observed some peculiar features of the events occurred Long Valley caldera regions, such as, i) a "burst" of high-frequency content at very small epicentral distances, ii) a long monotonic coda and iii) velocity spectra with a sharp dominant peak at 2Hz. On the contrary, VT earthquakes have characteristics quite similar to events occurred in shallow active crustal regions. Tusa and Langer (2016) observed that at Mount Etna different ground motion characteristics are observed for events occurred above and below a limit depth of 5km: the shallower earthquakes are more similar to LP earthquakes ("they have more low frequencies than deeper one"), while the deeper ones to the VT events. Further characteristics of volcanic events in Italy are: i) the attenuation with distance that can be faster than the shallow crustal earthquakes, according to macroseismic observations (Azzaro et al., 2006) and, more recently, to strong and weak motion recordings; ii) the large values of peak parameters and high-frequency amplitudes of records located very close to the source (Iervolino, 2019).

In the latest release of the hazard model of Italy (MPS04; Stucchi et al. 2011), the regional predictive equations used for volcanic areas were derived by De Natale et al. (1988) from weak-motion data recorded at the Campi Flegrei (Naples) and were applied to all the active volcanic districts in Italy. However, De Natale et al. (1988) only consists in scaling relationships of the peak parameters (PGA and PGV) with respect to seismic moment with a simple geometrical attenuation term (Montaldo et al., 2005). These features are apt to match the very fast amplitude decay from shallow earthquake sources, typical of volcanic regions. For the 2013 European Seismic Hazard Model (Woessner et al, 2015) the ground motion was predicted using the GMM developed by Faccioli et al. (2010), although not specifically derived for volcanic areas.

More recently, empirical ground motion equations having a functional form accounting for source, attenuation and site effect have been derived for the Mount Etna region by Tusa and Langer (2016). In their study, they used two separate functional forms for shallow (depth < 5 km) and deep (depth > 5 km) earthquakes. The model was then revised by Peruzza et al (2017), with a focus on shallow events and the adoption of the hypocentral distance.

In other areas of the world characterized by volcanic events, the situation is similar to Italy, since very few models are calibrated from empirical data. Munson and Thurber (1997) provide an empirical relation for the peak ground acceleration for the volcanic earthquakes in the Hawaiian Islands, whereas McVerry et al (2006) propose coefficients for the correction of the GMMs to account for

volcanic areas in New Zealand. Similarly to McVerry et al (2006), Atkinson (2010) proposes coefficients for the correction of the model by Boore and Atkinson (2008) for shallow crustal earthquakes in active tectonic regions. The study is based on the residual analysis that model the discrepancies between ground-motion observations for Hawaii and the reference GMM.

Following the recent earthquakes in the Mount Etna (mainshock 26/12/2018 $M_w=4.9$) area and in the island of Ischia (mainshock 21/08/2017 $M_w = 3.9$), it was possible to increase the number of recordings for volcanic areas in Italy and, in particular, to increase the number of observations close to the epicentre. The data revealed the limitations of previous models and especially their inadequacy to predict the ground motion observed in the near source. These are the reasons why we considered the opportunity to calibrate a new empirical model to predict the amplitudes of several intensity measures relevant for engineering applications, i.e. the PGA, PGV and the 5% damping acceleration spectral amplitudes (SA) in the vibration period interval $T=0.025-5s$. The new data allowed to robustly extend the magnitude range of pre-existing models to 4.9 and, following Tusa and Langer (2016), to include different attenuation with distance for shallow and deep events. We also consider the necessity to estimate the uncertainty related to the mean prediction, to provide useful elements to implement the backbone approach for a seismic hazard assessment (Douglas, 2018; Weatherill et al. 2018), which can be applicable in case of volcanic areas, where data are generally scarce.

2. Dataset

The dataset for volcanic zones in Italy contains waveforms from both accelerometers and broadband instruments of events with magnitude in the range 3.0 - 4.9 occurred in the Mount Etna and the Aeolian Islands plus one event occurred in Ischia in 2017 in the time span 2001-2019. We include the Ischia event because Michelini et al. (2017) showed how the model by Tusa and Langer (2016) reasonably predicts the spectral amplitudes of the 2017 M_w 3.9 Ischia earthquake for distance larger than 20km, while a bias is observed in the near source conditions. Moreover, Azzaro et al. (2006) showed as the attenuation decay with distance of Mt. Etna and Ischia island are very similar.

The strong-motion parameters have been obtained from the waveforms available at the Italian Accelerometric Archive (ITACA, <http://itaca.mi.ingv.it>; Luzi et al. 2008; Pacor et al. 2011). The dataset is composed of 615 waveforms relative to 41 events recorded by 155 stations.

The data comes from the records of the networks managed by the Italian Department of Civil Protection (Rete Accelerometrica Nazionale [RAN], code **IT**, doi:10.7914/SN/IT) and by the Istituto Nazionale di Geofisica e Vulcanologia (INGV; Italian National Seismic Network [INSN], code **IV**, doi:10.13127/SD/X0FXnH7QfY). The minor contribution comes from the network **MN** (Mediterranean Network [MEDNET] project, doi:10.13127/SD/fBBBtDtd6q), also managed by INGV. Since several accelerometric and broadband instruments are co-located for IV network, we keep in the dataset the broadband records, if records from both instruments are available, in order to avoid oversampling. All the waveforms were uniformly processed using the strong-motion processing tool the Engineering Strong Motion database (ESM, <http://esm.mi.ingv.it/processing/>; Puglia et al. 2018), according to the procedure described by Paolucci et al. (2011).

The location and magnitude of the events occurred at Mount Etna are revised according to the location of INGV Etna Observatory (OE) seismic catalogue (<http://sismoweb.ct.ingv.it>; Alparone et al. 2015); in the other cases, revised event metadata of INGV Italian Seismological Instrumental and Parametric Database catalogue (ISIDE, <http://iside.rm.ingv.it>) are used. If the moment magnitude M_w is not

available, we consider the local magnitude M_L as an alternative, without converting from one to the other. As a matter of fact, the dataset is mainly composed by low magnitude events for which the difference between the two metrics are quite small. Moreover, Luzi et al. (2014) showed as the introduction of a magnitude conversion could result in an increase of the standard deviation of a model calibrated over the data.

Considering that the maximum moment magnitude of the dataset is 4.9 and that fault geometries are generally not available for events with M_w smaller than 5.5, we adopt as a distance metric the hypocentral distance, R_{hyp} , rather than the distance from the fault rupture, R_{rup} .

A shear wave velocity V_S profile with depth is measured for about 13% of the recording stations; in the remaining cases the average velocity in the uppermost 30m, $V_{S,30}$, is inferred from the topographic slope, according to Wald and Allen (2007) model. On the basis of $V_{S,30}$ values, the sites are then classified according to the subsoil categories proposed by the Eurocode 8 (CEN, 2003).

The flatfile (parametric table) of the dataset is provided in the electronic supplement (ESUPP1) of this paper and is prepared according to the structure of the Engineering Strong Motion flatfile (ESM flatfile; Lanzano et al. 2019a). The user manual is available at <http://esm.mi.ingv.it/flatfile-2018/>, after registration.

Table 1 focuses on the characteristics of the very recent events occurred in 2017 and 2018, which correspond to about 20% of the dataset.

Table 1. Volcano earthquakes with $M > 3.5$ (M_L or M_w) occurred in Italy after 2016.

Event	Area	#records	M_L	M_w	h [km]
2017-08-21 18:57:50	<i>Ischia</i>	39	3.6	3.9	1.5
2018-10-06 00:34:19	<i>Etna</i>	47	4.7	4.6	4.5
2018-12-24 12:08:55	<i>Etna</i>	5	4.0		2.1
2018-12-24 19:26:18	<i>Etna</i>	4	4.0		2.1
2018-12-26 02:19:17	<i>Etna</i>	33	4.8	4.9	<5.0*
2019-01-08 23:50:34	<i>Etna</i>	2	4.1		2.2

* the metadata provided by INGV webservice are still preliminary (last access 06/02/2019)

Figure 1 shows the geographic distribution of epicentres in the Mount Etna and Aeolian islands regions and their magnitude and depth distributions. The shallow events ($h \leq 5$ km) are mainly located in the south-eastern flank of the volcano in a densely urbanized area, while the deep events ($h \geq 15$ km) in the north-western area, closest to the top of the volcano. The seismicity in the Aeolian Islands is instead sparse. The Ischia earthquake (not showed here) has been located in the Casamicciola Terme municipality in the proximity of the epicentre of the historical destructive event of 28/07/1883 (M_w 4.26).

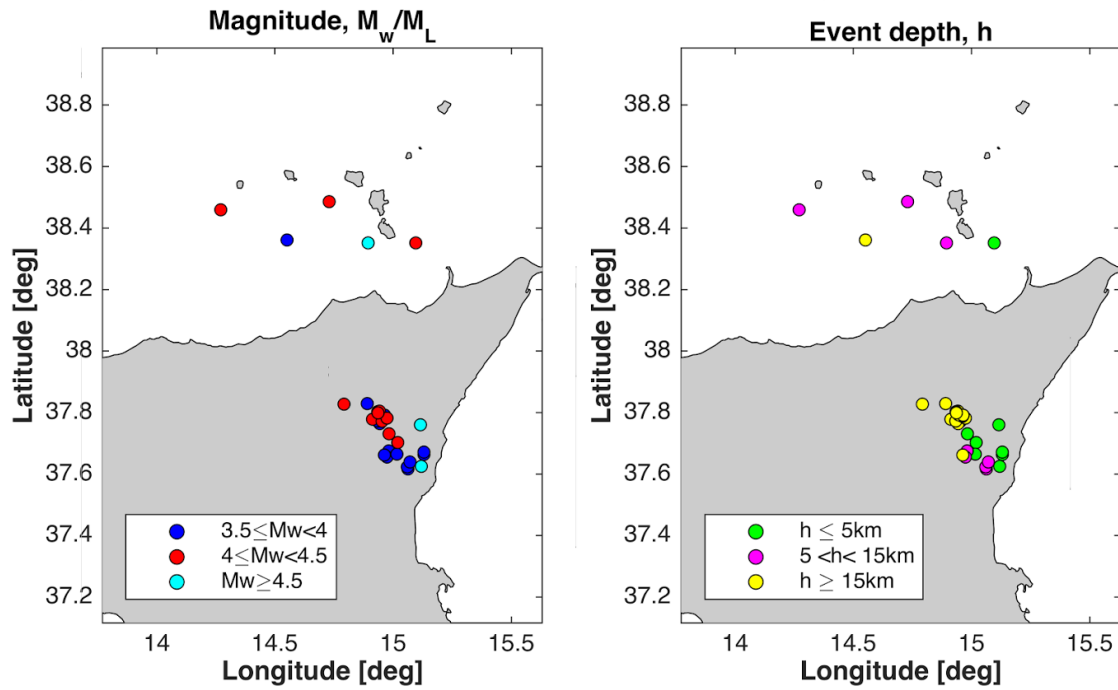


Figure 1. Map showing the location of the events. Left: magnitude; right: focal depth.

Figure 2 shows the distribution of (moment or local, if not available) magnitudes and hypocentral distances of the dataset. The data sampling is good in the magnitude range 3.5 - 4.9 and in the hypocentral distances from 20 to 120km. The number of data recorded at very short distances from the source is not negligible (about 40 records) and allows us to calibrate the model near the source. The empirical data at epicentral distances lower than 5km are 3: the record of the Ischia earthquake (21/08/2017 M_w 3.9) at the IV station Casamicciola (station code IOCA) with maximum $PGA=0.28g$ ($R_{epi}=0.9km$); the record of the Viagrante (Etna) earthquake (26/12/2018 M_w 4.9) at the IT station Santa Venerina (station code SVN) with maximum $PGA=0.55g$ ($R_{epi}=4.5km$); the record of the Etna earthquake (08/01/2019 M_L 4.1) at the IV station Monte Conca (station code EMCN) with maximum $PGA=0.12g$ ($R_{epi}=1.2km$).

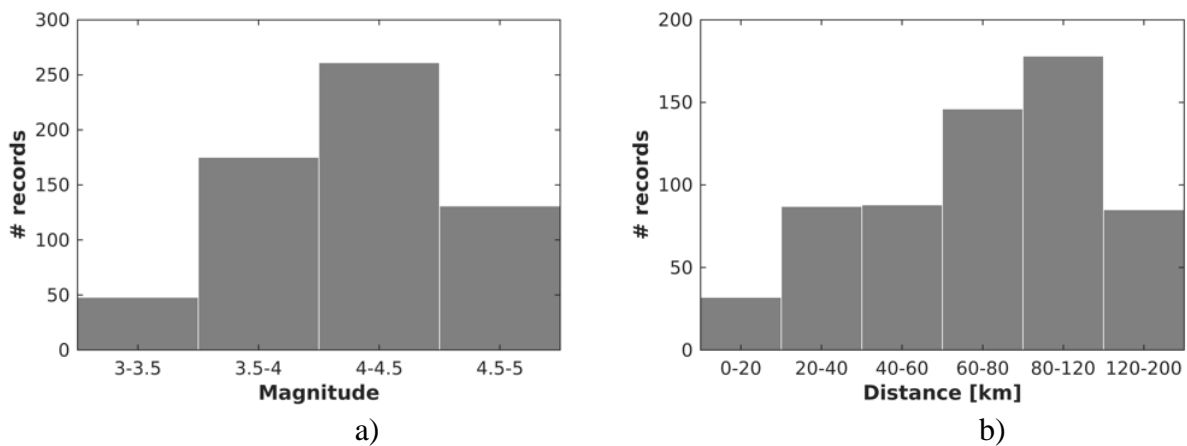


Figure 2. a) distribution of the records as a function of magnitude; b) distribution of the records as a function of the hypocentral distance.

Figure 3a shows the magnitude-distance distribution of the records and reveals that the near source records are relevant to all magnitudes. Figure 3b reports the number of records as a function of periods, divided by Eurocode 8 (EC8) site categories. The number of usable records decreases with increasing vibration period as a function of the high-pass corner frequency adopted in the waveform processing, which is, on average 0.1Hz, but for analogue records is usually higher (about 0.25Hz). Following Boore and Bommer (2005), no record selection is carried out for the low-pass at high frequencies. A strong reduction of records number is evident after 5s, that is selected as the upper limit for the GMM calibration.

Sites of EC8-A ($V_{s,30} > 800\text{m/s}$) and EC8-B ($360\text{m/s} < V_{s,30} < 800\text{m/s}$) categories are properly represented in the dataset, while the number of records of EC8-C ($180\text{m/s} < V_{s,30} < 360\text{m/s}$) sites is remarkably smaller. The record number of categories EC8-D ($V_{s,30} < 180\text{m/s}$) and EC8-E (soil layer of type EC8-C or -D with a thickness from 5 to 20m and underlain by rock with $V_{s,30} > 800\text{m/s}$) is almost negligible.

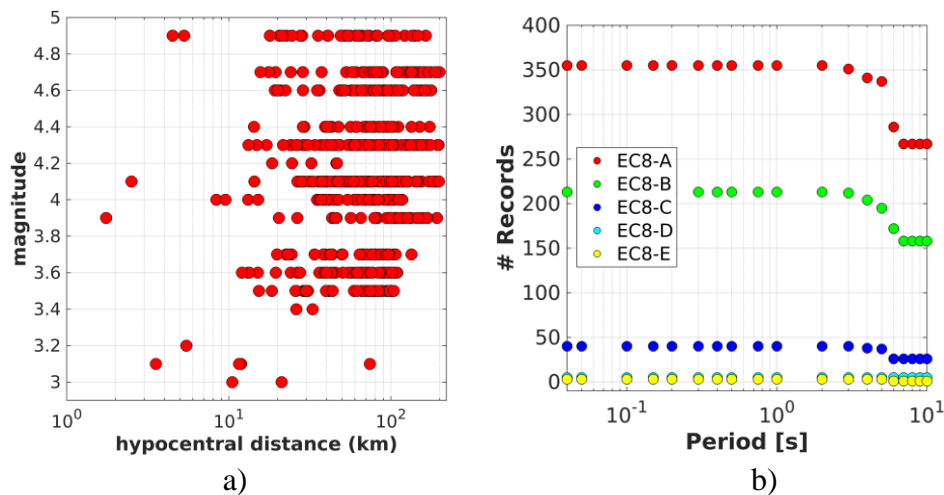
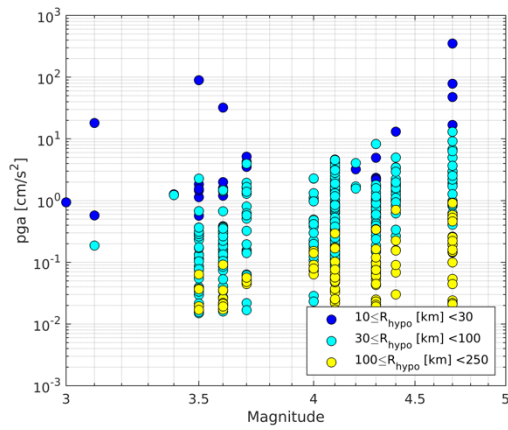


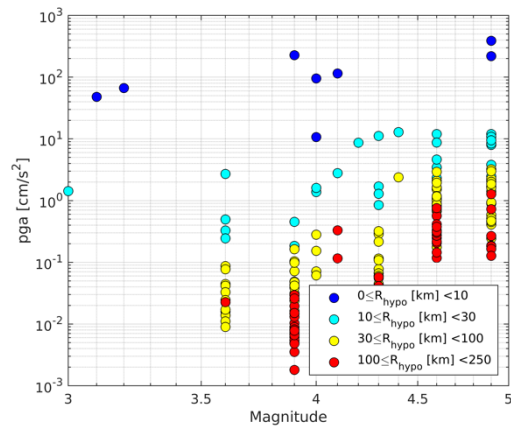
Figure 3. a) magnitude-distance distribution of the records; b) number of usable records as a function of period, separated by EC8 soil categories.

As previously discussed, volcanic earthquakes show different characteristics in relation to depth. Figure 4 shows the data scaling with magnitude of PGA and SA at $T=1\text{s}$, for different distance classes divided in deep ($h > 5\text{km}$) and shallow ($h \leq 5\text{km}$) events, respectively. Similarly, Figure 5 shows the scaling with distance of the same parameters for different magnitude classes. The plots of Figure 4 and 5 for SA at $T=0.2$ and 2s are provided in the Electronic supplement (ESUPP2).

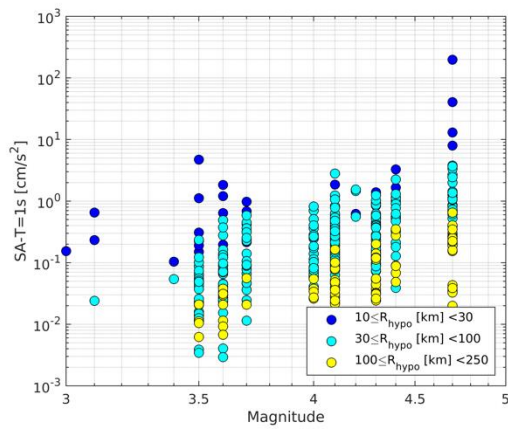
The trend with magnitude does not seem to be affected by depth and a linear dependence on magnitude is observed for both short (PGA) and long periods (Figure 4). This most likely depends on the maximum magnitude of the dataset, which is 4.9, since, usually, the saturation of ground motion is observed for magnitude larger than 6. On the other hand, the attenuation with distance has significantly different trends in case of deep or shallow events. The short period ground motion generated by deep events shows slower attenuation and evidence of anelastic attenuation (Figure 5a). On the other hand, shallow events show a stronger attenuation of the ground motion, even at very short distances, and a negligible contribution of anelastic attenuation (Figure 5b). A magnitude-dependent attenuation of ground motion, which is usually visible for magnitudes greater than 5, is not clearly observed. Similar considerations can be carried out concerning the attenuation with distance at long periods, although the differences between surface and deep earthquakes are smaller.



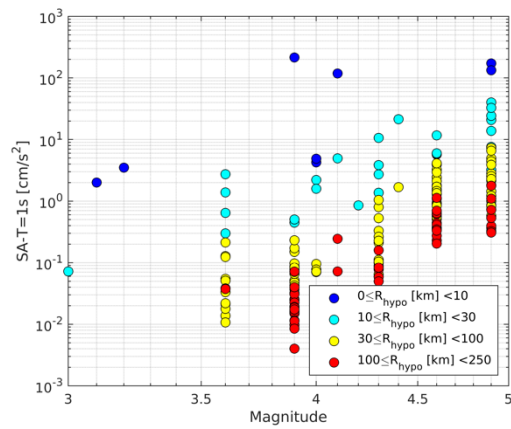
a)



b)



c)



d)

Figure 4. a) PGAs vs. magnitude for different distance classes (deep earthquakes $h > 5 \text{ km}$); b) PGAs vs. magnitude for different distance classes (shallow earthquakes $h \leq 5 \text{ km}$); c) SA amplitudes at $T=1 \text{ s}$ vs. magnitude for different distance classes (deep earthquakes $h > 5 \text{ km}$); d) SA amplitudes at $T=1 \text{ s}$ vs. magnitude for different distance classes (shallow earthquakes $h \leq 5 \text{ km}$).

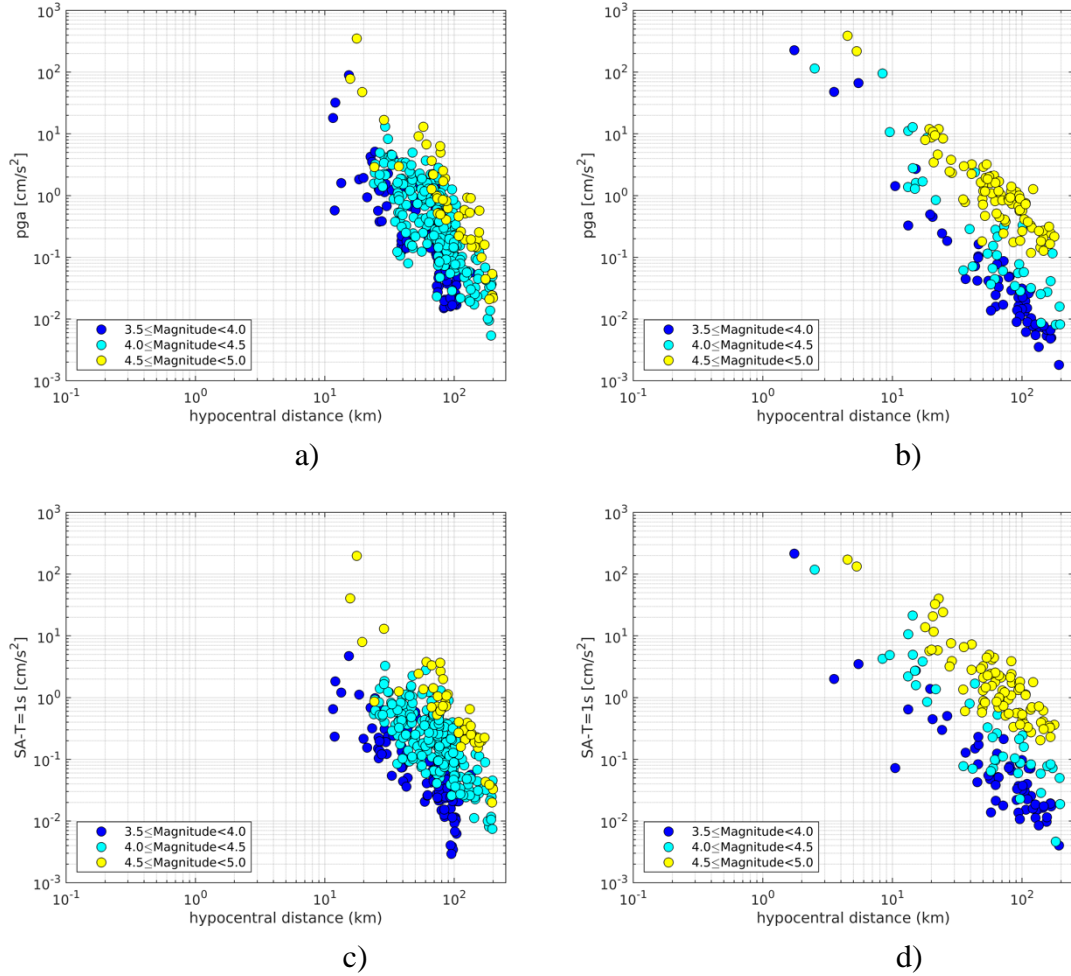


Figure 5. a) PGAs vs. hypocentral distance for different classes of magnitude (deep earthquakes $h > 5\text{km}$); b) PGAs vs. hypocentral distance for different classes of magnitude (shallow earthquakes $h \leq 5\text{km}$); c) SA amplitudes at $T=1\text{s}$ vs. hypocentral distance for different classes of magnitude (deep earthquakes $h > 5\text{km}$); d) SA amplitudes at $T=1\text{s}$ vs. hypocentral distance for different classes of magnitude (shallow earthquakes $h \leq 5\text{km}$).

We test the performance of the existing empirical models against the dataset. In particular, the local model by Tusa and Langer (2016), hereinafter TL16, and the global model proposed by Faccioli et al. (2010), named FAC10, are selected. TL16 is expressed in terms of epicentral distance and is valid up to 100km; FAC10 is calibrated for R_{rup} and is valid up to 200 km. Figure 6 reports the total residuals R_{es} (i.e. the logarithmic difference of observations and predictions) as a function of distance, considering PGA and SA at $T=1\text{s}$ as intensity measures. **The plots for SA at $T=0.2$ and 2s are available in the ESUPP2.** For TL16 predictions, we consider the functional form by Sabetta and Pugliese (1996) for shallow events ($h \leq 5\text{km}$) and the one by Boore and Atkinson (2008) for the deep ones ($h > 5\text{km}$). Positive residuals result in under-predictions, while negative residuals in over-predictions.

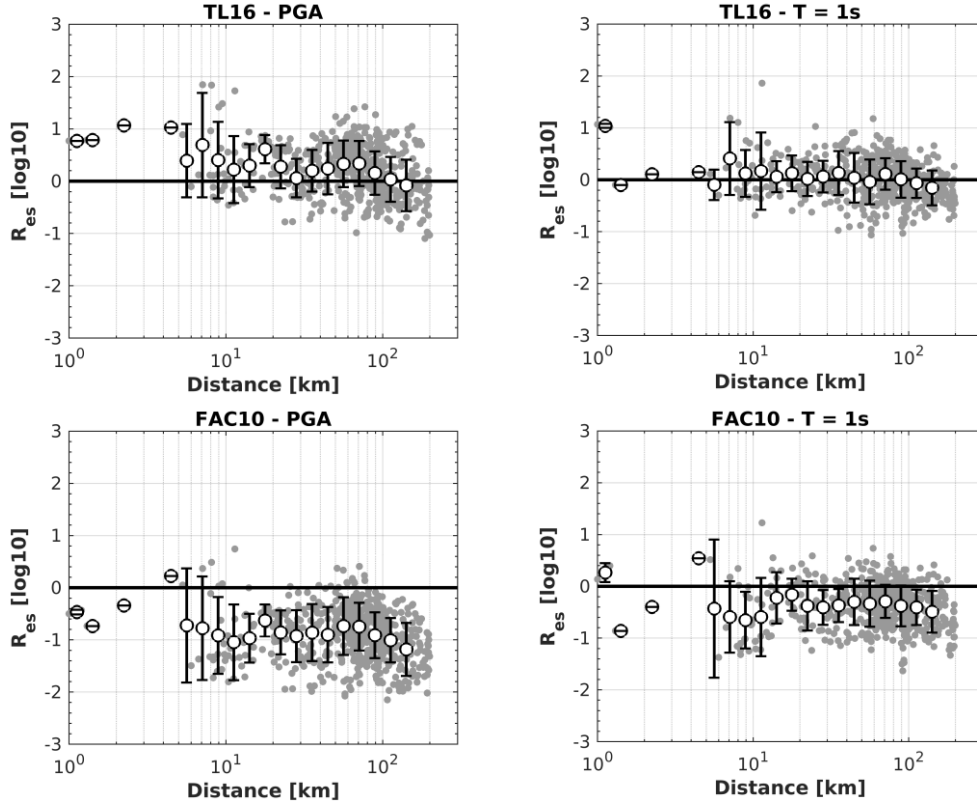


Figure 6. Total residuals of the models: top) Tusa and Langer (2016); bottom) Faccioli et al. (2010). Left: PGA; right: spectral ordinates at T=1s.

TL16 has positive residuals at distances lower than 10-20km, while residuals have nearly zero-mean at larger distances, both for PGA and SA-T=1s. On the contrary, the model by Faccioli et al. (2010) well predicts the near-source data but shows large negative PGA residuals at distances larger than 10km. The analyses confirm that none of the models examined is able to describe the ground motion recorded considering all distances and depths. In particular, TL16 significantly underestimates (about 10 times) the ground motion in near source for shallow events, since the recent observations indicate that the high-frequency intensity measures have larger values than crustal events. Considering the importance for the seismic hazard of the predictions at a very short distance, the derivation of a new model is needed.

3. Model calibration

The observations made in previous section lead us to construct a functional form in which the ground-motion dependence on magnitude is linear, the geometrical attenuation is only dependent on distance and the effect of anelastic attenuation is accounted for only in case of deep events.

The proposed functional form is:

$$\log_{10}Y = a + bM + F_D + F_S + \delta B_e + \delta S2S_s + \delta W_{0,es} \quad (1)$$

Where a is the offset and M is the moment magnitude. The term distance F_D is:

$$F_D = \begin{cases} c_1 \log_{10} \sqrt{R_{hyp}^2 + h_1^2} & \text{focal depth } h \leq 5 \text{ km} \\ c_2 \log_{10} \sqrt{R_{hyp}^2 + h_2^2} + c_3 \sqrt{R_{hyp}^2 + h_2^2} & \text{focal depth } h > 5 \text{ km} \end{cases} \quad (2)$$

where R_{hyp} is the hypocentral distance and the pseudo-depth is equal to $h_1=2\text{km}$ for shallow earthquakes and $h_2=5\text{km}$ for deep events.

The site term is $F_S=s_i$ with $i=1,2,3$. In particular, $i=1$ corresponds to rock sites belonging to the subsoil category EC8-A ($s_1=0$), $i=2$ for sites of class EC8-B and $i=3$ for sites of class EC8-C and -D.

Alternative approaches (Zhao et al. 2006; Laouami et al. 2018) for site categorization were found to be more effective to describe the site-effects, but, for the purposes of this study, we adopt a classification scheme, as much as possible, consistent with the European and Italian Building codes.

The least squares calibration was performed with a linear mixed-effect model in which the coefficients a , b , c_1 , c_2 , c_3 , s_1 , s_2 and s_3 represent the fixed part, while the total residuals were decomposed in event- δB_e and site- $\delta S_2 S_s$ terms (random terms), whose standard deviations are τ and $\phi_{S_2 S_s}$, respectively. σ_0 is the residual aleatory variability (standard deviation of event- and site-corrected residuals). The total sigma σ is obtained as:

$$\sigma = \sqrt{\tau^2 + \phi_{S_2 S_s}^2 + \sigma_0^2} \quad (3)$$

The model (hereinafter LL19) is calibrated for the geometric mean of the horizontal components of PGA (cm/s^2), PGV (cm/s) and 30 ordinates of SA (from $T = 0.025\text{s}$ to $T = 5\text{s}$). The coefficients of the regression are listed in Table 2. The coefficients independent from the IM/period are $s_1=0$; $h_1=2\text{ km}$; $h_2=5\text{ km}$. In particular, the pseudo-depths were obtained from preliminary non-linear regressions and the averaged values over periods are set as constants in the final linear regression.

Table 2. Coefficients of the predictive model for volcanic events (LL19).

IMs	a	b	c ₁	c ₂	c ₃	s ₂	s ₃	τ	$\phi_{S_2 S_s}$	σ_0
PGA	-0.4185	0.8146	-2.0926	-1.5694	-0.0062	0.0880	0.3382	0.1892	0.2624	0.2215
SA-T=0.025s	-0.3849	0.8113	-2.0995	-1.5689	-0.0063	0.0866	0.3373	0.1887	0.2644	0.2228
SA-T=0.04s	-0.2622	0.7983	-2.1271	-1.5777	-0.0065	0.0861	0.3306	0.1908	0.2725	0.2246
SA-T=0.05s	-0.1428	0.7870	-2.1536	-1.5859	-0.0069	0.0863	0.3323	0.1955	0.2846	0.2284
SA-T=0.07s	0.0810	0.7714	-2.2186	-1.5859	-0.0076	0.0774	0.3139	0.2039	0.3078	0.2392
SA-T=0.1s	0.4160	0.7293	-2.2624	-1.6135	-0.0075	0.0609	0.2997	0.2164	0.3240	0.2312
SA-T=0.15s	0.2806	0.7569	-2.2177	-1.5882	-0.0069	0.0714	0.3465	0.2193	0.3204	0.2155
SA-T=0.2s	0.0339	0.8028	-2.1606	-1.5803	-0.0060	0.0716	0.3297	0.2200	0.3039	0.2126
SA-T=0.25s	-0.2205	0.8577	-2.1228	-1.5948	-0.0052	0.0512	0.3204	0.1995	0.2837	0.2101
SA-T=0.3s	-0.4404	0.8872	-2.0652	-1.5829	-0.0047	0.0752	0.3468	0.1932	0.2726	0.2053
SA-T=0.35s	-0.6916	0.9169	-2.0099	-1.5577	-0.0042	0.0838	0.3818	0.1838	0.2607	0.2043
SA-T=0.4s	-1.0431	0.9744	-1.9542	-1.5409	-0.0038	0.0820	0.3672	0.1850	0.2576	0.2034
SA-T=0.45s	-1.2374	1.0111	-1.9411	-1.5544	-0.0038	0.0878	0.3882	0.1794	0.2467	0.2053
SA-T=0.5s	-1.3532	1.0303	-1.9337	-1.5871	-0.0034	0.1033	0.4053	0.1736	0.2461	0.2039
SA-T=0.6s	-1.6118	1.0629	-1.8831	-1.6015	-0.0029	0.1161	0.4056	0.1681	0.2336	0.2006
SA-T=0.7s	-1.9639	1.1092	-1.8177	-1.5795	-0.0027	0.1086	0.4195	0.1550	0.2300	0.1974
SA-T=0.75s	-2.0659	1.1181	-1.7968	-1.5618	-0.0029	0.1159	0.4277	0.1581	0.2314	0.1950
SA-T=0.8s	-2.1093	1.1189	-1.7961	-1.5741	-0.0027	0.1174	0.4371	0.1541	0.2289	0.1944
SA-T=0.9s	-2.2763	1.1315	-1.7722	-1.5776	-0.0023	0.1212	0.4374	0.1552	0.2287	0.1885

SA-T=1s	-2.5171	1.1553	-1.7230	-1.5615	-0.0018	0.1201	0.4480	0.1496	0.2279	0.1904
SA-T=1.2s	-2.6980	1.1748	-1.7111	-1.6079	-0.0013	0.1195	0.4313	0.1595	0.2286	0.1865
SA-T=1.4s	-2.9144	1.1842	-1.6536	-1.5777	-0.0015	0.1155	0.4136	0.1846	0.2217	0.1855
SA-T=1.6s	-3.0714	1.2011	-1.6641	-1.6102	-0.0013	0.1269	0.3770	0.1953	0.2226	0.1823
SA-T=1.8s	-3.1426	1.1967	-1.6553	-1.6305	-0.0012	0.1337	0.3756	0.1888	0.2221	0.1793
SA-T=2s	-3.2273	1.1995	-1.6524	-1.6597	-0.0009	0.1440	0.3917	0.1929	0.2187	0.1824
SA-T=2.5s	-3.4744	1.2057	-1.6227	-1.6420	-0.0011	0.1388	0.3712	0.2060	0.2111	0.1850
SA-T=3s	-3.7121	1.2118	-1.5741	-1.6063	-0.0012	0.1261	0.3836	0.2356	0.2139	0.1825
SA-T=3.5s	-3.4558	1.1198	-1.5393	-1.6194	-0.0011	0.1101	0.3639	0.2506	0.2098	0.1816
SA-T=4s	-3.5044	1.0943	-1.4949	-1.6025	-0.0012	0.1064	0.3447	0.2442	0.2093	0.1832
SA-T=4.5s	-3.3949	1.0490	-1.4750	-1.6088	-0.0011	0.0908	0.3587	0.2287	0.1952	0.1835
SA-T=5s	-3.4022	1.0258	-1.4711	-1.6097	-0.0011	0.0856	0.3386	0.2273	0.1954	0.1835
PGV	-2.5366	0.9809	-1.8482	-1.5676	-0.0042	0.0995	0.3747	0.1433	0.2126	0.2099

The total variability (Eq. 3) is in the range 0.33-0.45 in logarithmic decimal units. These values are very similar to the standard deviations obtained by Tusa and Langer (2016) and Peruzza et al. (2017), that are in the range 0.33-0.44 in logarithmic decimal units. On the other hand, the standard deviations are generally higher than the ones obtained for active crustal regions (e.g. Bindi et al. 2011; Lanzano et al, 2019b). This increase in variability may reflect the peculiarity of volcanic events, since the location and magnitude estimation have larger uncertainties than in case of tectonic events. In addition, the classification of sites is challenging, due to the large variability in the stiffness of volcanic deposits and rocks and the paucity of geophysical tests.

A sanity check of the regression results is performed in Figure 7, which compares the magnitude term $F_M = bM$ with the residuals of PGA and SA at T=1s, after the removal of the systematic event and site terms. The graphs of Figure 7 of SA at T=0.2s and 2s are available in the ESUPP2. As expected, a larger scatter is observed in the PGA residuals with respect to SA at T=1s.

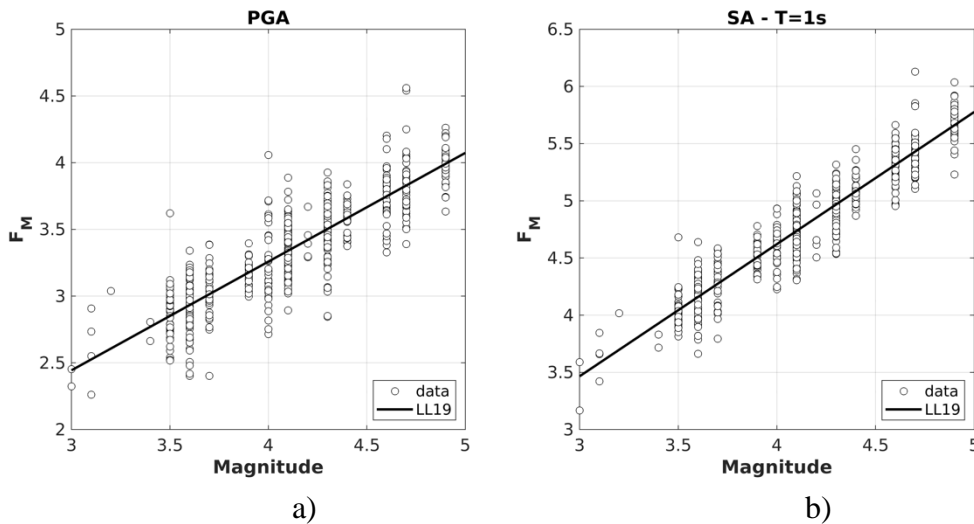


Figure 7. Magnitude term $F_M = bM$ against site- and source- corrected residuals: a) PGA; b) SA – T=1s.

Figure 8 shows the scaling of LL19 with the distance ($M_w = 4.5$) for the shallow and deep events against the corrected residuals for the same parameters of Figure 7. The graphs show that the attenuation for shallow and deep events is remarkably different at low periods and for PGA, while, at longer periods, the attenuation term has more similar trend.

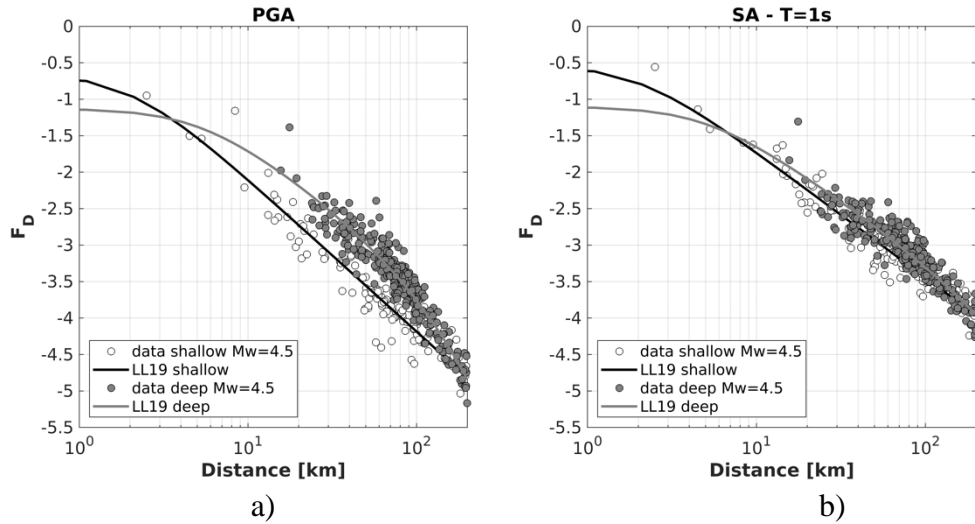


Figure 8. Distance term of Eq. (1) against site- and source- corrected residuals for $M_w=4.5$: a) PGA; b) SA – $T=1s$. Empty circles are observations of shallow events; grey filled circles are observations of deep events.

In Figure 9 the site-effect terms obtained in the LL19 calibration for stiff (s_2) and soft soil (s_3) sites and those provided for the most recent shallow active crustal GMMs in Italy, i.e. the model by Bindi et al. (2011), named ITA10, and the very recent model by Lanzano et al. (2019), named ITA18. The latter, in particular, is calibrated on a considerably larger dataset with respect to ITA10 (about 5 times).

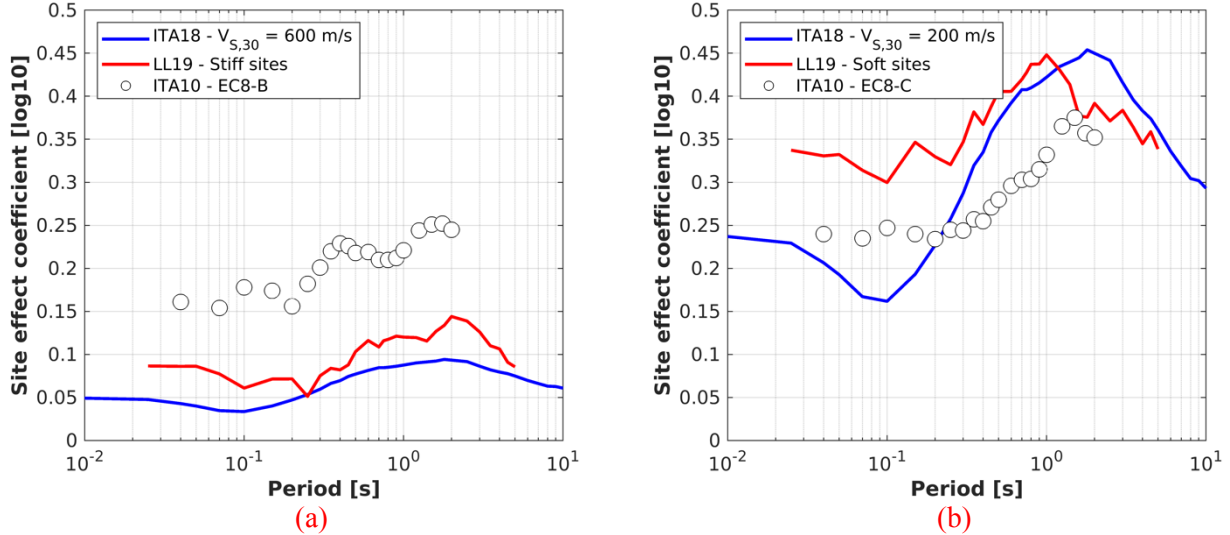


Figure 9. Site coefficients of LL19 (this study), ITA18 (Lanzano et al. 2019b) and ITA10 (Bindi et al. 2011): a) stiff soil sites; b) soft soil sites.

The comparison shows that LL19 have a reasonable agreement with ITA18, especially for the stiff soil sites; for the soft sites LL19 the coefficient for site amplification is found to be larger at short periods. We compute two statistical indexes to check i) the significance of the addition these terms in the model and ii) the uncertainty in the prediction. In the first case, we consider, as indicator, the *p-Value* (Wasserstein and Lazar, 2016): low *p-Values* (< 0.05) indicate a meaningful addition to the model because changes in the predictor's value are related to changes in the response variable. For LL19, the *p-Value* of the coefficient for stiff and soft soils are on average 0.08 and 0.001, respectively.

Concerning the goodness of fit, we consider the Standard Error (*SE*) associated to site effects coefficients. *SE* associated to soft soil sites predictions (on average 0.09) is almost 2 times larger than those observed for stiff sites (0.05). The latter findings indicate that the introduction in the GMMs functional form of the term for soft soils is more important than that for stiff soils, despite of the prediction uncertainty is larger.

Figure 10a to 10d show the plot of the within-event average error as a function of hypocentral distance and the between-event error as a function of magnitude for PGA and SA-T=1s (same plots for SA-T=0.2 and 2s in ESUPP2). The site- and event- corrected residuals, $\delta W_{0,es}$ (obtained by removing the epistemic part of the uncertainty), are mostly in the range $\pm 0.5 \log_{10}$ units, whereas the between-event error generally is in the range $\pm 0.3 \log_{10}$ units, numbers in agreement with ITA10 and ITA18.

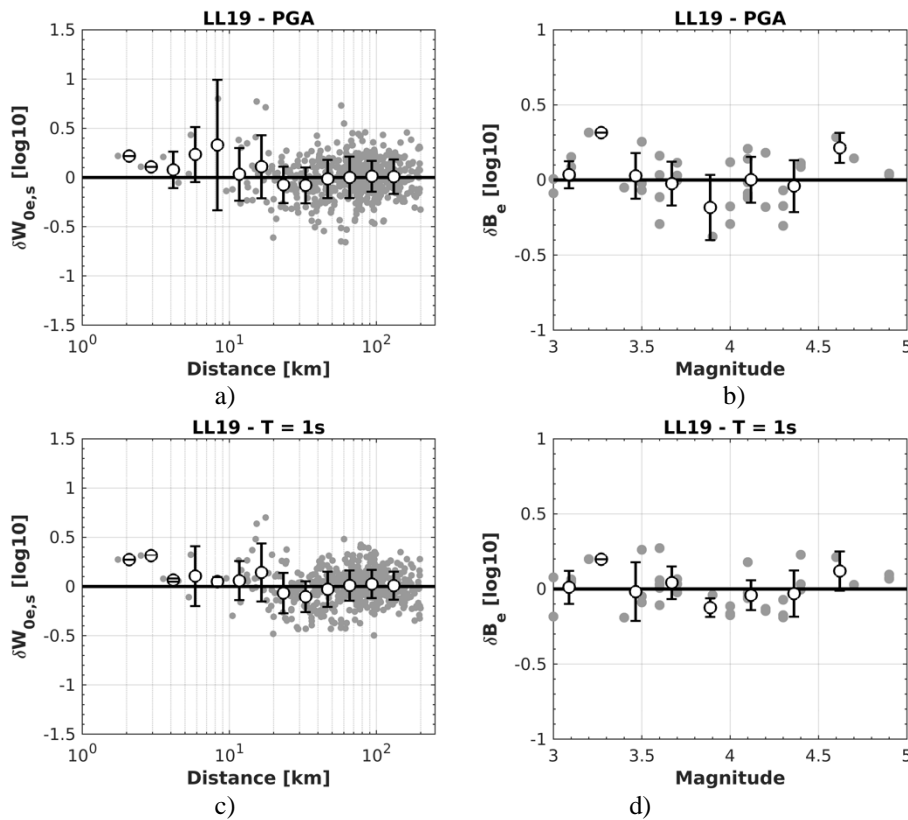


Figure 10. Residuals of the proposed model: a) site- and source- corrected residuals as a function of hypocentral distance (PGA); b) between-event as a function of magnitude (PGA); c) site- and source-corrected residuals as a function of hypocentral distance (T=1s); d) between-event errors as a function of magnitude (T=1s).

In the Figures 11 and 12 we compare the model and the observations of two significant events of the dataset, namely the M_w 3.9 Ischia earthquake (21 August 2017) and the M_w 4.9 Viagrande earthquake (26 December 2018). The graphs also show the predictions by Faccioli et al. (2010) and Peruzza et al. (2017); the latter, named TL16 hypo, was calibrated with data up to 100km. The model calibrated in this study reproduces accurately the observations, especially in the case of the Viagrande earthquake. The observations of the Ischia earthquake are slightly underpredicted in case of PGA and rock and stiff soil sites.

Considering the most relevant magnitude-distance scenarios for seismic hazard assessment, the three models predict PGA values significantly different: for $M_w=3.9$, $R_{hypo}=1\text{km}$ and rock sites, the prediction of the proposed model is about 0.1g and is included between the PGA estimates of FAC10

and TL16, which are 0.34g and 0.02g, respectively (Figure 11a); when we move to $M_w=4.9$ (Figure 12a), the PGA of the proposed GMM is the largest (0.7g), while TL16 still predicts values, significantly lower than the other model (0.14g). Similar behaviors are observed at long periods and for the other site classes. At intermediate distances ($R_{\text{hypo}}=20\text{km}$) the PGA predictions of FAC10 are always significantly higher than the other models.

Additional plots, available in the electronic supplements (ESUPP3), compare the 5% damped acceleration response spectra of the records near and far from the source with the median \pm sigma spectra predicted by LL19, for the three site classes. The records are divided in near and far field, considering different discerning thresholds, corresponding to $R_{\text{hypo}}=20\text{km}$ for shallow events and $R_{\text{hypo}}=50\text{km}$ for deep events. The LL19 predictions are calculated considering the median values of each magnitude-distance interval considered. In general, the comparison of predictions and experimental observations is good both for shallow and deep events, although the data for each subset are very few in some cases.

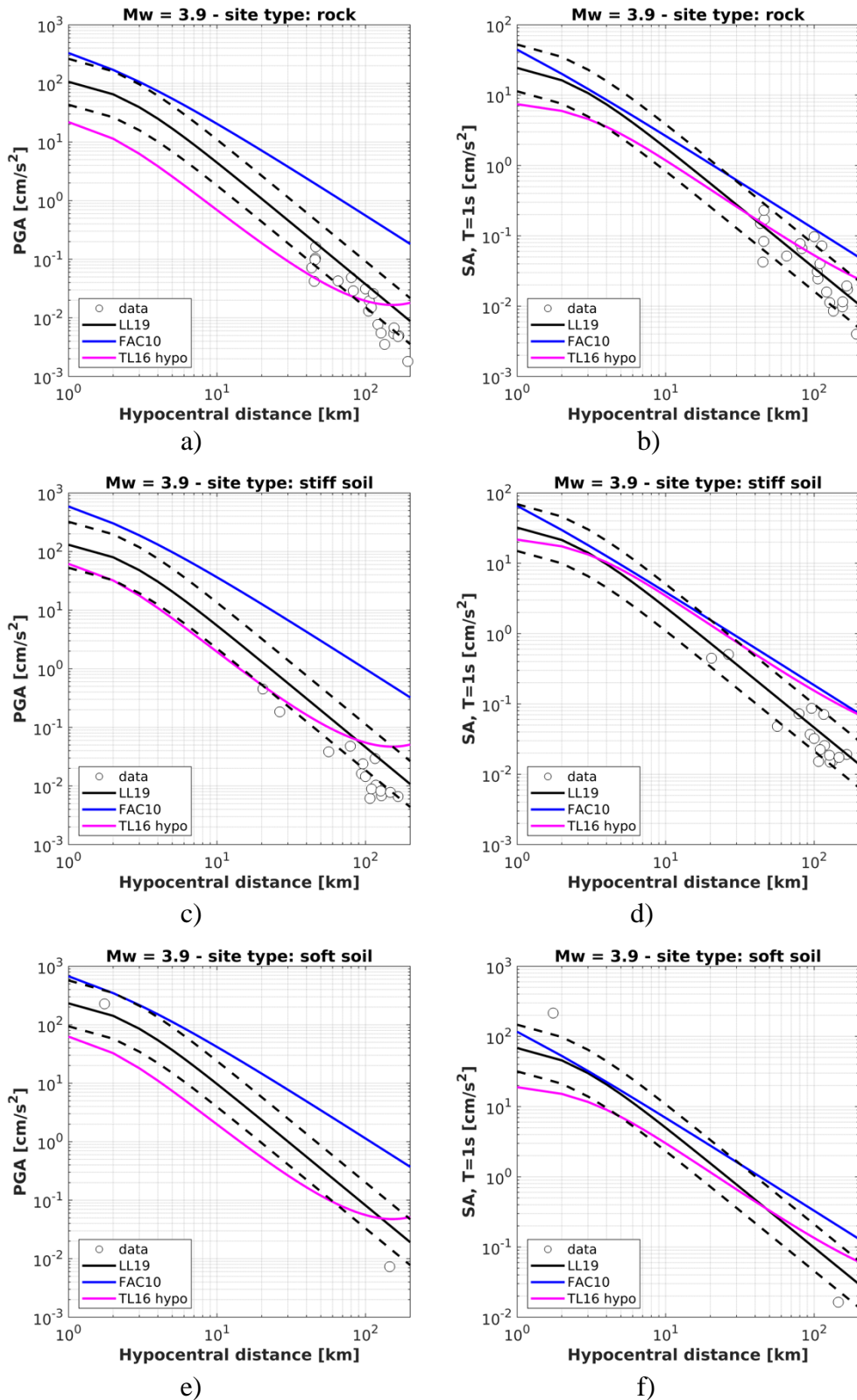


Figure 11. Comparison between ground motion models and observations of the 21/08/2017 Ischia earthquake (M_w 3.9) for rock sites (EC8-A), in the upper panel, stiff soils (EC8-B), in the central panel and soft soils (EC8-B and -C), in the lower panel. PGA is shown in the left column and SA $T=1s$ in the right column, and *GMPE shallow* is the model calibrated in this work for shallow events, *TL16 hypo* is the model by Peruzza et al. (2017) and *FAC10* is the model by Faccioli et al. (2010). **The black dotted lines are the LL19 predictions +/- 1 standard deviation.**

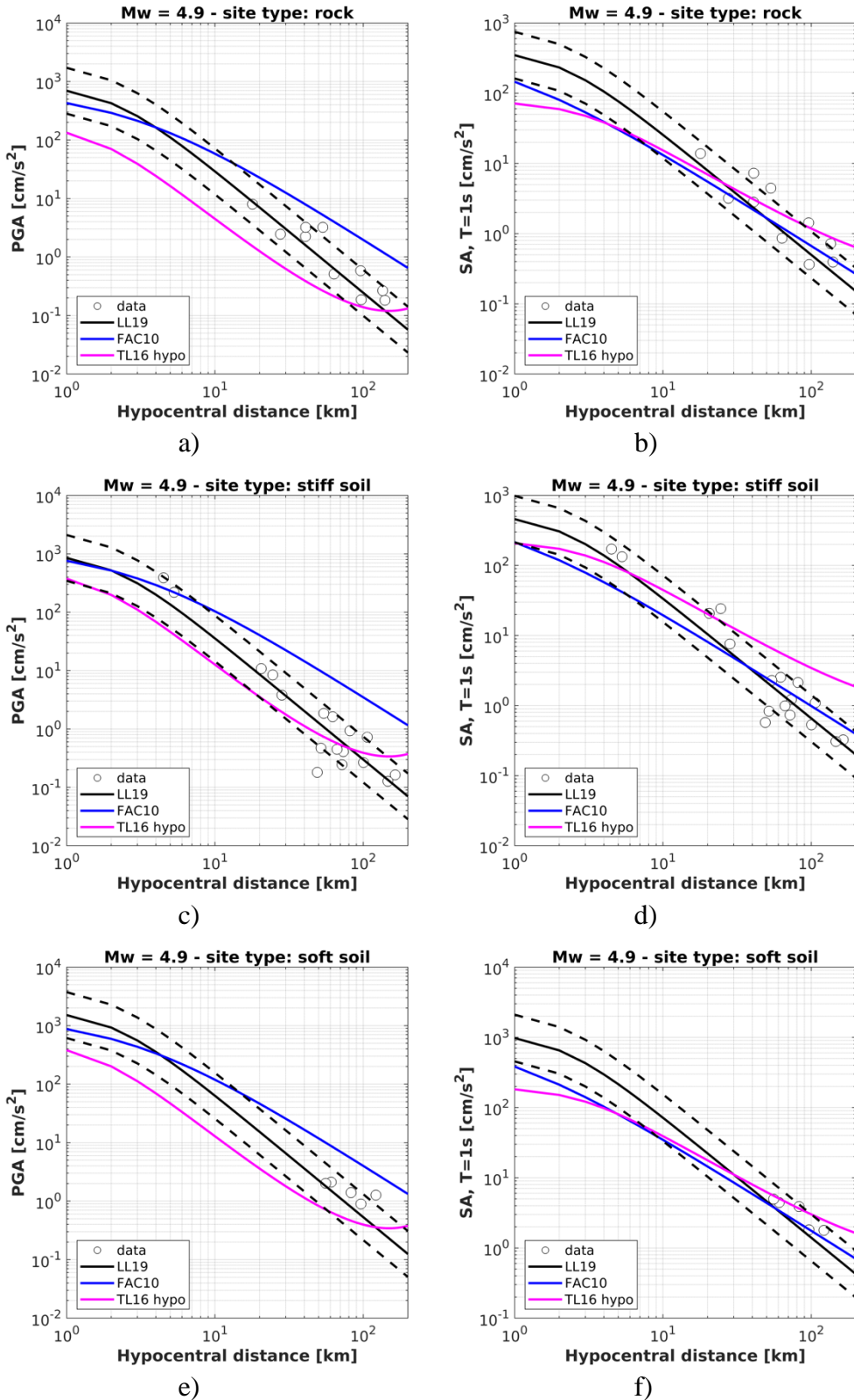


Figure 12. Comparison between ground motion models and observations of the Viagrande earthquake of 26/12/2018 (MW 4.9) for rock sites (EC8-A), in the upper panel, stiff soils (EC8-B), in the central panel and soft soils (EC8-B and -C), in the lower panel. PGA is shown in the left column and SA T=1s in the right column. (b, d and f) for rock sites (EC8-A), stiff soils (EC8-B) and soft soils (EC8-B and -C). *GMPE shallow* is the model calibrated in this work for shallow events, *TL16 hypo* is the model by Peruzza et al. (2017) and *FAC10* is the model by Faccioli et al. (2010). The black dotted lines are the LL19 predictions +/- 1 standard deviation.

4. Epistemic uncertainty

Recent approaches to build up logic trees for probabilistic seismic assessment (Petersen et al. 2014; Douglas, 2018) model the epistemic uncertainty of the ground motion prediction as the model-to-model differences or on the base of the statistics of the model fits and empirical data distributions, while accounting for imposed model constraints (Al Atik and Youngs, 2014). The latter represents the minimum uncertainty to be used with the models and is generally provided by the GMMs developers. This part of the epistemic uncertainty σ_μ can be calculated as (Al Atik & Youngs 2014; Bindi et al. 2017, 2019; Lanzano et al. 2019b):

$$\sigma_\mu = \sqrt{J_0^T [\text{varCov}_{x_i}] J_0} \quad (4)$$

where x_i represents the data points used to develop the model, J_0 is the Jacobian matrix, i.e. the gradient of the model with respect to its coefficients, evaluated in the predictive “location” x_0 , and varCov_{x_i} is the variance-covariance matrix of the coefficients, evaluated at all data points x_i .

Figure 13 shows the trend σ_μ as a function of moment magnitude, hypocentral distance and period; the dependence of σ_μ with respect to focal depth and site categories is also reported. If not specified, σ_μ is calculated for $M_w=4.0$, $R_{hyp}=10\text{km}$ and rock sites. In general, we observe that σ_μ is lower for shallow events ($h \leq 5\text{km}$) with respect to deep events, especially for magnitudes lower than 4.5. As already observed by other authors (Al-Atik et al. 2014; Bindi et al. 2017) σ_μ is strongly dependent on magnitude, where the highest values are at the extremes of the validity range and the minimum is at $M=4.0$. σ_μ is larger at short distances and it is mainly due to the limited amount of data available for the model calibration. Finally, the errors associated with the predictions of soft soil sites are larger than those obtained for stiff soils and rock. The trend of σ_μ with period shows a peak around 0.1s, which is the period affected by the largest aleatory variability in most of the empirical models in the literature. Finally, as expected, the values of σ_μ are larger than those proposed for Italian shallow crustal earthquakes by Lanzano et al. (2019b), who calibrated the model with about 10 times the number of data used in this study.

The values of σ_μ are provided in the electronic supplement (**ESUPP4**) as a Matlab 5D matrix (*s_mu.mat*), σ_μ is a function of the intensity measure, moment magnitude, hypocentral distance, focal depth and site category. An informative document (**ESUPP5**) for the usage of the **ESUPP4** is provided.

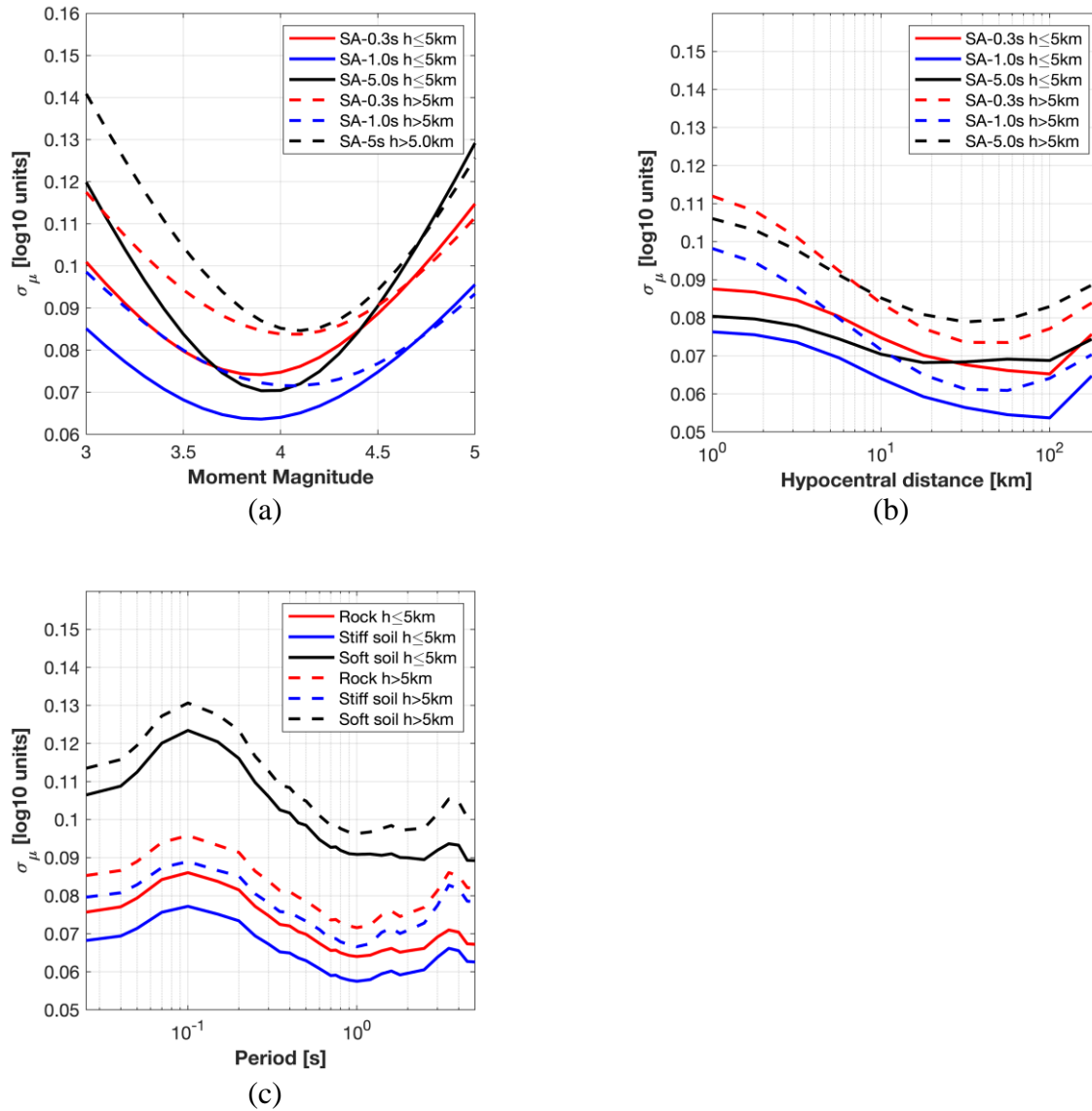


Figure 13. Epistemic uncertainty σ_μ , as a function of (a) moment magnitude M_w ($R_{hyp}=10\text{km}$, rock sites), (b) hypocentral distance R_{hyp} ($M_w=4.0$, rock sites) and (c) vibration period, T ($R_{hyp}=10\text{km}$, $M_w=4.0$).

5. Conclusions

According to the historical catalogue of seismicity in Italy (e.g. Parametric Catalog of Italian Earthquakes, CPTI15, <https://emidius.mi.ingv.it/CPTI15-DBMI15/>), earthquakes caused by volcano activities can have the same dangerous effects of those occurring in shallow active crustal regions. As a matter of fact, in Italy the active volcanoes are located in very densely populated areas (e.g. Catania and surroundings, Campi Flegrei, Vesuvius), where strong events could cause fatalities and the damage of strategic infrastructures. On the other hand, there are very few GMMs for the prediction of ground motion in volcanic areas, mostly because observations are scarce and volcanic earthquakes are generally rare.

The recent observations of earthquakes occurred in volcanic districts in Italy (Mount Etna 2018-2019 sequence; Ischia Island 2017 sequence) nonetheless showed that the seismic ground motion in the vicinity of the source is characterized by high values of ground motion parameters, larger than the

amplitudes of the design spectrum prescribed by the Italian seismic design code (returning period 475 years) for a broader range of periods (Iervolino, 2019). In fact, in case of a shallow event of moderate magnitude (e.g. M_w 4.9 Viagrande, on 24 December 2018) it has been observed a PGA of the order of 0.6g.

A new GMM is calibrated from a dataset tailored to the active volcanoes areas in Italy, so that it can be used in the future release of the seismic hazard models or for shakemap calculations. We use a single functional form with two different distance terms for shallow and deep events, in order to better constrain the magnitude scaling and the site coefficients. The magnitude range is about 3.0-5.0 and the hypocentral distance range is 1-200km. The GMM is valid for geometrical mean of the horizontal components of PGA and several amplitudes of the acceleration spectra, 5% damping, in the period interval $T=0.025$ -5s. We also estimate the error associated to the median prediction, so that it can be used as epistemic uncertainty in logic trees of the probabilistic analysis of seismic hazard.

Acknowledgments

The strong-motion dataset used in this article was built in the framework of the programme of the new hazard model for Italy, named MPS19, by the Seismic Hazard Center (Centro di Pericolosità Sismica) of the Istituto Nazionale di Geofisica e Vulcanologia (INGV). The authors would like to acknowledge the coordinators of the MPS19 programme, Carlo Meletti and Warner Marzocchi, and the co-coordinator of Task 4 (Ground Motion Models), Vera D'Amico. The authors are part of the ITACA (ITalian ACcelerometric Archive) team at INGV Milano and are grateful to the other members of the team (Francesca Pacor, Rodolfo Puglia, Maria D'Amico, Chiara Felicetta, Sara Sgobba and Emiliano Russo) for their fundamental support.

Reference

- Al Atik L, Youngs RR (2014) Epistemic uncertainty for NGA-West2 models. *Earthq Spectra* 30(3):1301–1318.
- Alparone S, Maiolino V, Mostaccio A, Scaltrito A, Ursino A, Barberi G, D'Amico S, Di Grazia G, Giampiccolo E, Musumeci C, Scarfi L, Zuccarello L (2015) Instrumental seismic catalogue of Mt. Etna earthquakes (Sicily, Italy): ten years (2000-2010) of instrumental recordings. *Annals of Geophysics* 58(4):0435.
- Atkinson GM (2010) Ground-motion prediction equations for Hawaii from a referenced empirical approach. *Bull Seismol Soc Am* 100(2):751-761.
- Azzaro R, Barbano MS, D'Amico S, Tuvè T (2006) The attenuation of seismic intensity on the Etna region and comparison with other Italian volcanic districts. *Annals of Geophysics* 49(4/5): 1003-1020.
- Bindi D, Pacor F, Luzi L, Puglia R, Massa M, Ameri G, Paolucci R (2011) Ground motion prediction equations derived from the Italian strong motion database. *Bull Earthq Eng* 9(6): 1899-1920.
- Bindi D, Cotton F, Kotha SR, Bosse C, Stromeyer D, Grünthal G (2017) Application-driven ground motion prediction equation for seismic hazard assessments in non-cratonic moderate-seismicity areas. *J Seismol* 21(5):1201–1218.

Bindi D, Kotha SR, Weatherill G, Lanzano G, Luzi L, Cotton F (2019) The pan-European Engineering Strong Motion (ESM) flatfile: consistency check via residual analysis. *Bull Earthq Eng* 17(2):583–602.

Boore DM, Bommer JJ (2005) Processing of strong-motion accelerograms: needs, options and consequences. *Soil Dyn Earthq Eng* 25(2): 93-115.

Boore DM, Atkinson GM (2008) Ground-motion prediction equations for the average horizontal component of PGA, PGV, and 5%-damped PSA at spectral periods between 0.01 s and 10.0 s. *Earthq Spectra* 24(1):99-138.

CEN (2004) EuroCode 8: design of structures for earthquake resistance—part 1: general rules, seismic actions and rules for buildings. European Committee for Standardization, Bruxelles.

De Natale G, Faccioli E, Zollo A (1988) Scaling of peak ground motions from digital recordings of small earthquakes at Campi Flegrei, southern Italy. *Pure Appl Geoph* 126(1):37-53.

Douglas J (2018) Capturing geographically-varying uncertainty in earthquake ground motion models or what we think we know may change, in *Recent Advances in Earthquake Engineering in Europe*. ECEE 2018, K. Pitilakis (Editor), Geotechnical, Geological and Earthquake Engineering, Vol. 46, Springer, Cham, Switzerland.

Faccioli E, Bianchini A, Villani M (2010) New ground motion prediction equations for $T > 1$ s and their influence on seismic hazard assessment. In *Proceedings of the University of Tokyo Symposium on Long-Period Ground Motion and Urban Disaster Mitigation*, Mar 2010.

Iervolino, I. (2019). Editoriale. Il moto al suolo nel terremoto di Viagrande (CT). *Progettazione Sismica*, (3) (in Italian).

Lanzano G, Sgobba S, Luzi L, Puglia R, Pacor F, Felicetta C, D'Amico M, Cotton F, Bindi D (2019a) The pan-European Engineering Strong Motion (ESM) flatfile: compilation criteria and data statistics. *Bull Earthq Eng* 17(2): 561–582.

Lanzano G, Luzi L, Pacor F, Felicetta C, Puglia R, Sgobba S, D'Amico M (2019b) A revised ground motion prediction model for shallow crustal earthquakes in Italy. *Bull Seismol Soc Am* 109 (2): 525-540.

Laouami N, Slimani A, Larbes S (2018) Ground motion prediction equations for Algeria and surrounding region using site classification based H/V spectral ratio. *Bull Earthq Eng* 16:2653-2684.

Luzi L, Hailemichael S, Bindi D, Pacor F, Mele F, Sabetta F (2008) ITACA (ITalian ACcelerometric Archive): A Web Portal for the Dissemination of Italian Strong-motion Data. *Seismol Res Lett* 79(5): 716–722.

Luzi L, Bindi D, Puglia R, Pacor F, Oth A (2014) Single-station sigma for Italian strong-motion stations. *Bull Seismol Soc Am* 104(1): 467-483.

McVerry GH, Zhao JX, Abrahamson NA, Somerville PG (2006) Crustal and subduction zone attenuation relations for New Zealand earthquakes. *Bull New Zeal Soc Earthq Eng* 39(1).

Michelini A, Luzi L, Lanzano G, Puglia R, Felicetta C, D'Amico M, Russo E, Pacor F, Faenza L, Lauciani V, Cultrera G, Milana G (2017). Il terremoto di Casamicciola del 21 agosto 2017: osservazioni sul moto del suolo. *INGV Terremoti blog* 14/09/2017. (<https://ingvterremoti.wordpress.com/2017/09/14/il-terremoto-di-casamicciola-del-21-agosto-2017-osservazioni-sul-moto-del-suolo/>) (in Italian).

Montaldo V, Faccioli E, Zonno G, Akinci A, Malagnini L (2005) Treatment of ground-motion predictive relationships for the reference seismic hazard map of Italy. *J Seismol* 9: 295–316.

Munson CG, Thurber CH (1997) Analysis of the attenuation of strong ground motion on the island of Hawaii. *Bull Seismol Soc Am* 87(4): 945-960.

Pacor F, Paolucci R, Luzi L, Sabetta F, Spinelli A, Gorini A, Nicoletti M, Marcucci S, Filippi L, Dolce M (2011) Overview of the Italian strong motion database ITACA 1.0. *Bull Earthquake Eng* 9(6): 1723–1739.

Paolucci R, Pacor F, Puglia R, Ameri G, Cauzzi C, Massa M (2011) Record processing in ITACA, the new Italian strong-motion database. In: Akkar S, Gu' lkan P, van Eck T (eds) Chapter 8 of the book *earthquake data in engineering seismology—predictive models, data management and networks*. ISBN: 978-94-007-0151-9 (printed version) 978-94-007-0152-6 (E-book version). *Geotechnical, geological, and earthquake engineering*, vol 14, Springer, Netherlands

Peruzza L, Azzaro R, Gee R, D'Amico S, Langer H, Lombardo G, Pace B, Pagani M, Panzera F, Ordaz M, Suarez ML, Tusa G (2017) When probabilistic seismic hazard climbs volcanoes: the Mt. Etna case, Italy—Part 2: Computational implementation and first results. *Natural Hazards Earth System Science* 17:1999-2015.

Petersen et al. 2014. Documentation for the 2014 update of the United States national seismic hazard maps, U.S. Geological Survey Open-File Report 2014-1091, 243pp.

Pitt AM, Hill DP (1994) Long- period earthquakes in the Long Valley Caldera region, eastern California. *Geoph Res Lett* 21(16): 1679-1682.

Puglia R, Russo E, Luzi L, D'Amico M, Felicetta C, Pacor F, Lanzano G (2018) Strong-Motion Processing Service: a tool to access and analyse earthquakes strong-motion waveforms. *Bull Earthquake Eng* 16(7): 2641–2651.

Sabetta F, Pugliese A (1987) Attenuation of peak horizontal acceleration and velocity from Italian strong-motion records. *Bull Seismol Soc Am* 77:1491–1513.

Stucchi M, Meletti C, Montaldo V, Crowley H, Calvi GM, Boschi E (2011) Seismic Hazard Assessment (2003-2009) for the Italian Building Code. *Bull Seismol Soc Am* 101(4): 1885–1911.

Tusa G, Langer H (2015) Prediction of ground motion parameters for the volcanic area of Mount Etna. *J Seismol* 20(1): 1–42.

Wald DJ, Allen TI (2007) Topographic slope as a proxy for seismic site conditions and amplification. *Bull Seismol Soc Am* 97(5):1379–1395

Wasserstein RL, Lazar NA (2016) The ASA's statement on p-values: Context, process, and purpose. *Am Stat* 70(2): 129–133.

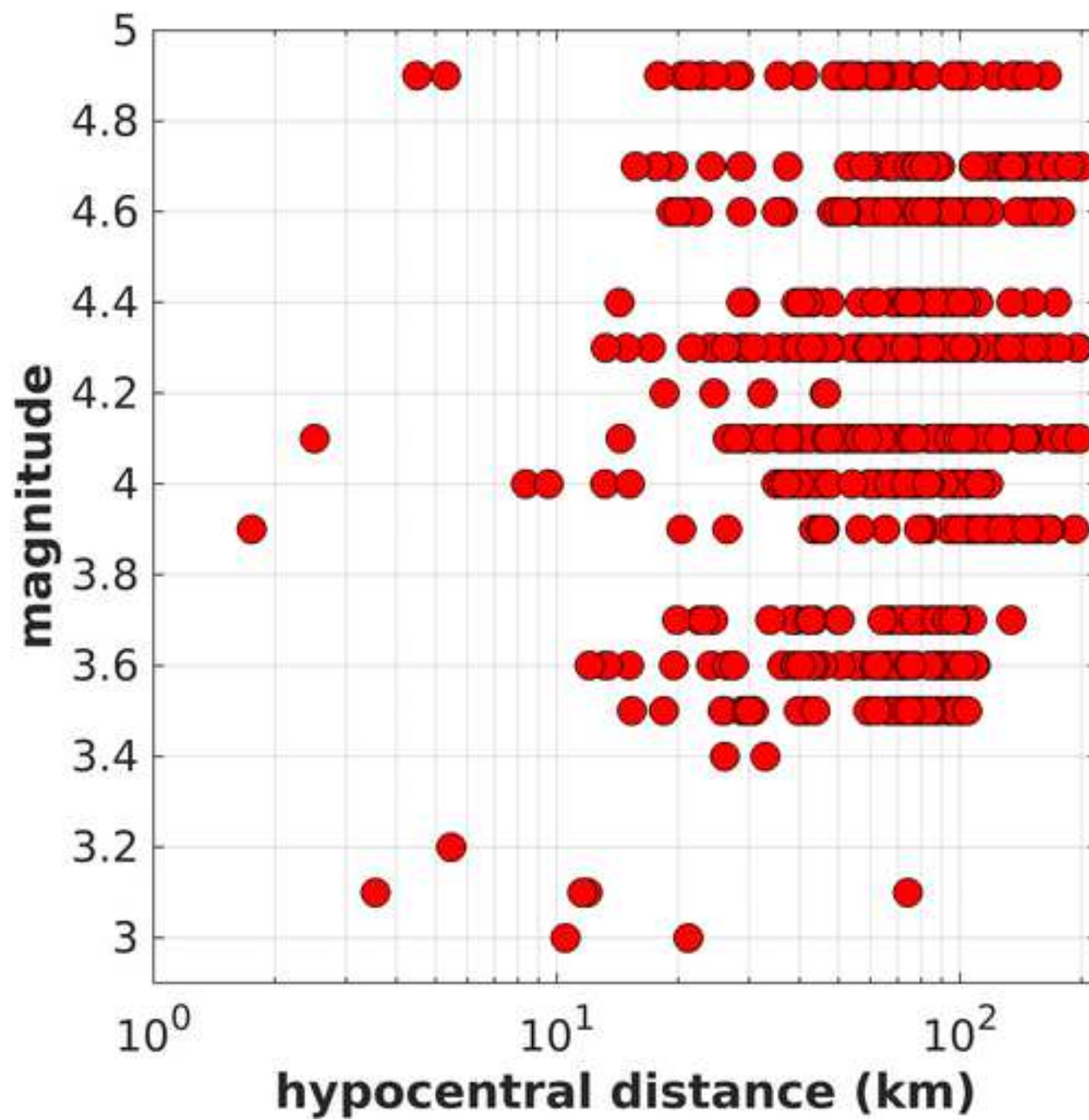
Weatherill G., Bindi D., Cotton F., Danciu L., Luzi L. (2018). Building a new ground motion logic tree for Europe: needs, challenges and new opportunities from European seismological data. In: *Proceedings of the 16th European Conference on Earthquake Engineering*, 18-21 June, Thessaloniki, Greece.

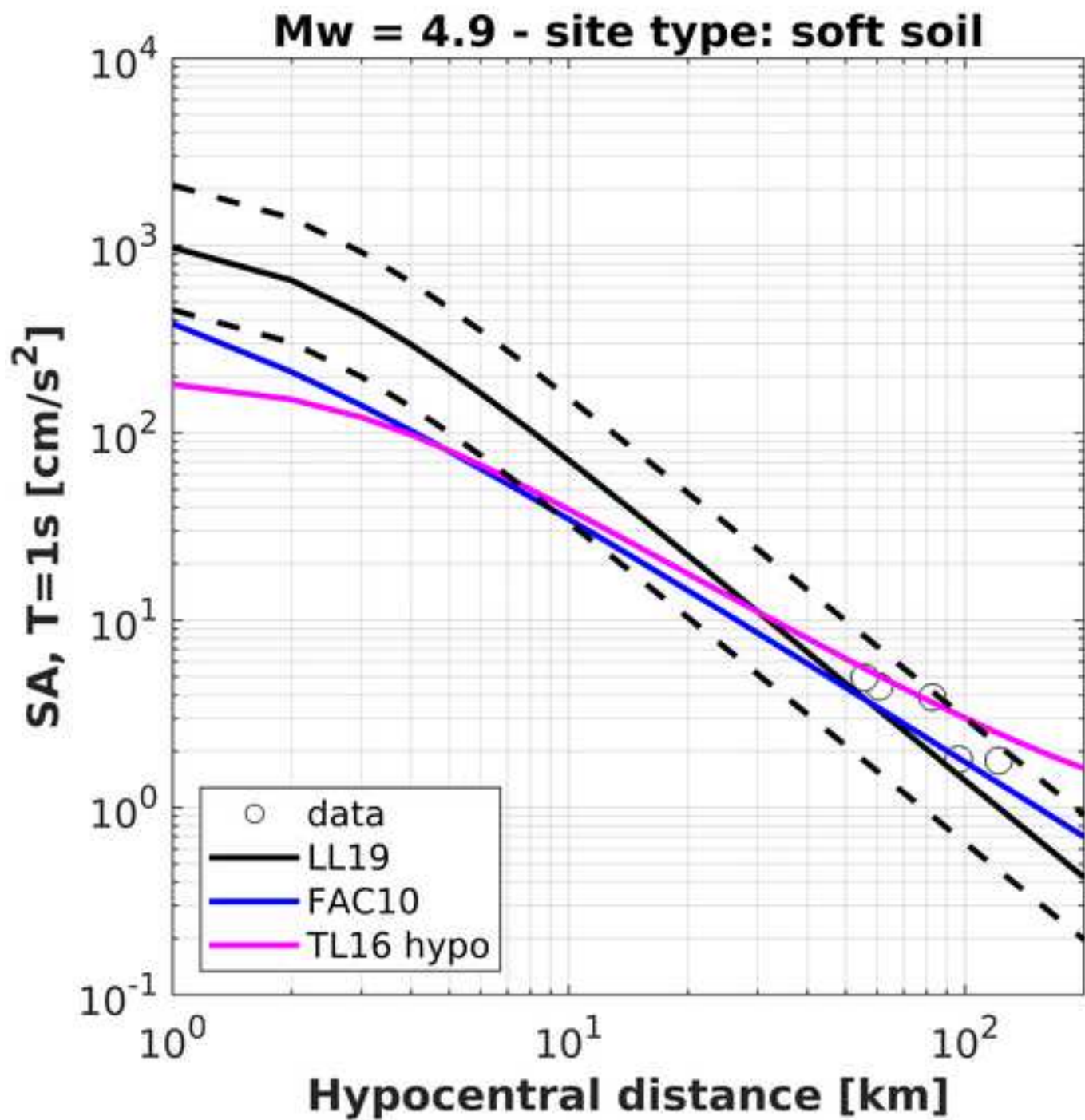
Woessner J, Laurentiu D, Giardini D, Crowley H, Cotton F, Grünthal G, Valensise G, Arvidsson R, Basili R, Demircioglu MB, Hiemer S, Meletti C, Musson RW, Rovida AN, Sesetyan K, Stucchi M (2015) The 2013 European seismic hazard model: key components and results. *Bull Earthq Eng* 13(12):3553–3596.

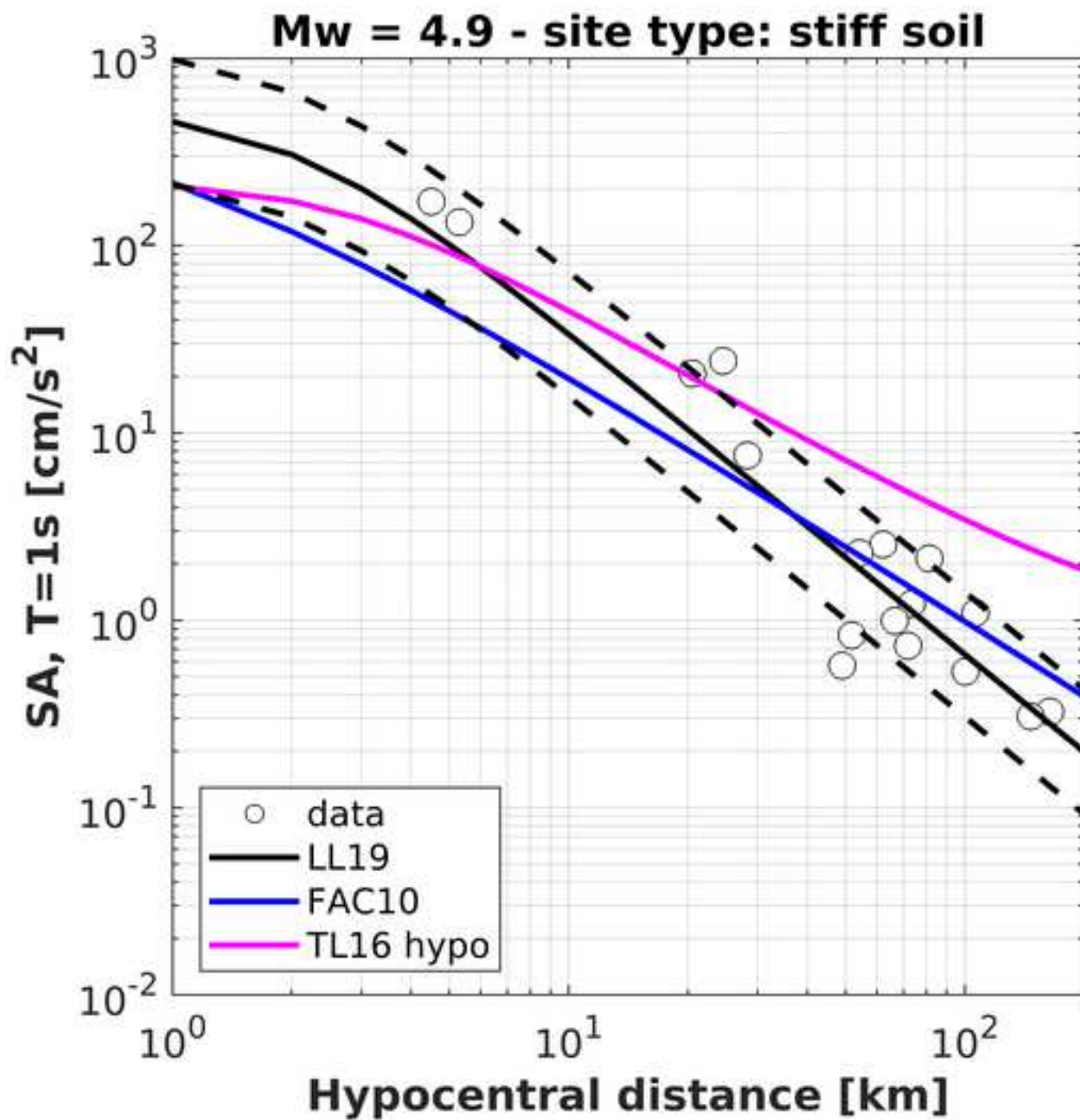
Zhao JX, Irikura K, Zhang J, Fukushima Y, Somerville PG, Asano A, Ohno Y, Oouchi T, Takahashi T, Ogawa H (2006). An empirical site classification method for strong-motion stations in Japan using H/V response spectral ratio. *Bull Seismol Soc Am* 96:914-925.

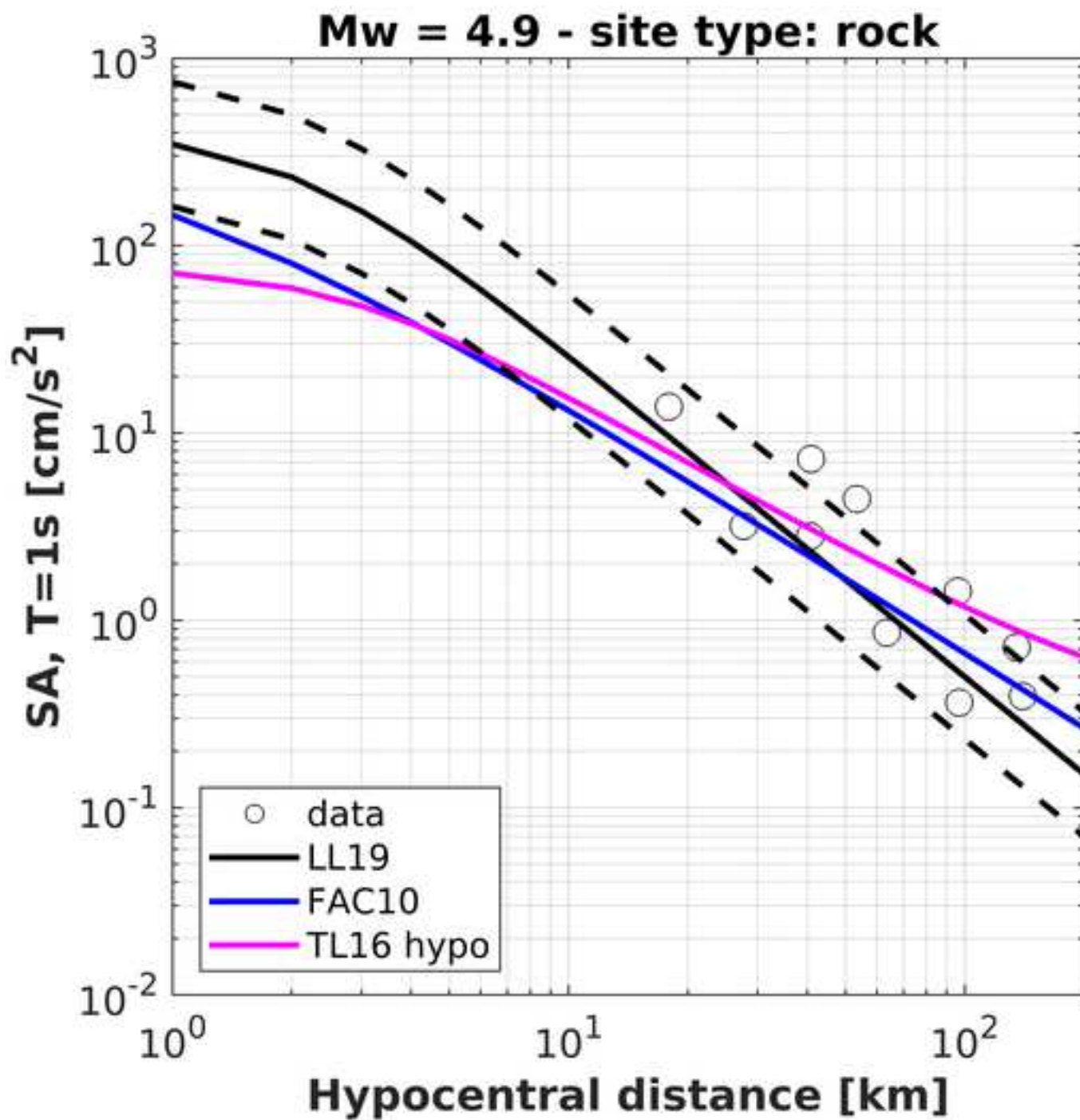
Electronic supplementary material:

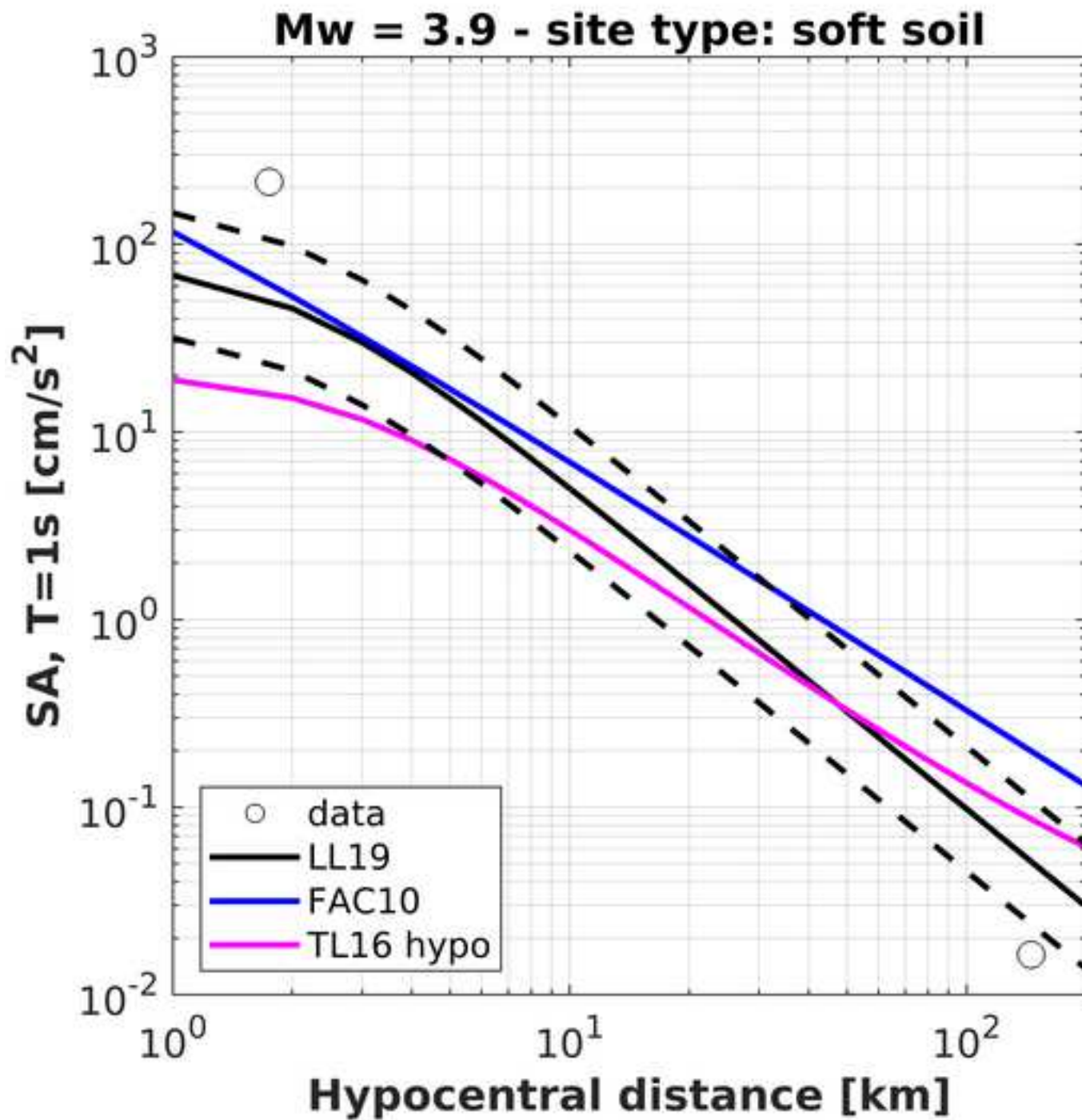
- ESUPP1: flatfile of the dataset of volcanic earthquakes in Italy (esupp.csv)
- ESUPP2: Figures 4, 5, 6, 7, 8 and 10 of the paper for SA at T=0.2 and 2s (esupp2.pdf)
- ESUPP3: comparison of observed and LL19 predictions of 5% damping acceleration response spectra (esupp3.pdf)
- ESUPP4: Matlab 5D array with error associated with GMMs predictions (s_mu.mat)
- ESUPP5: read_me.txt for the usage of s_mu.mat

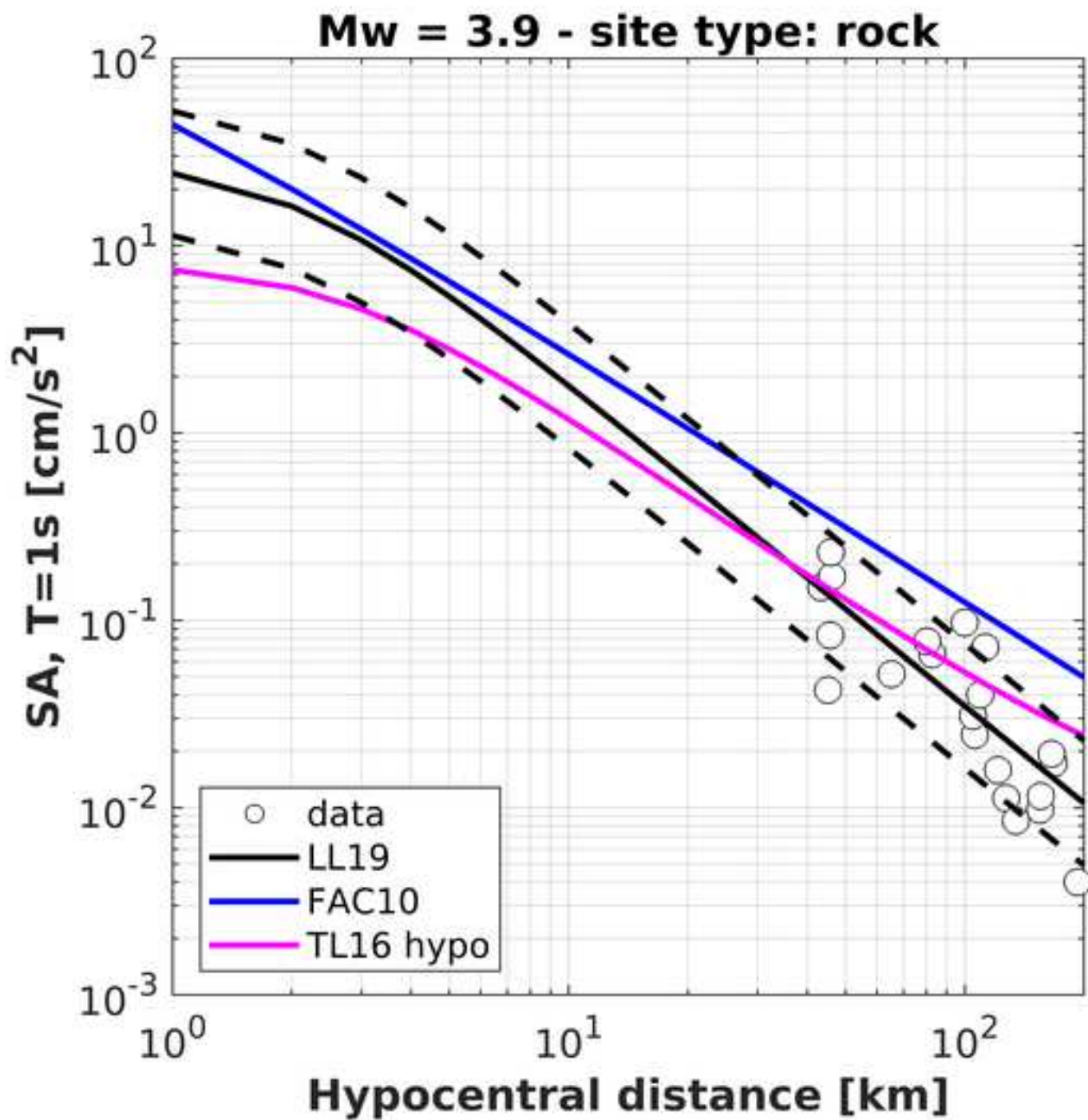


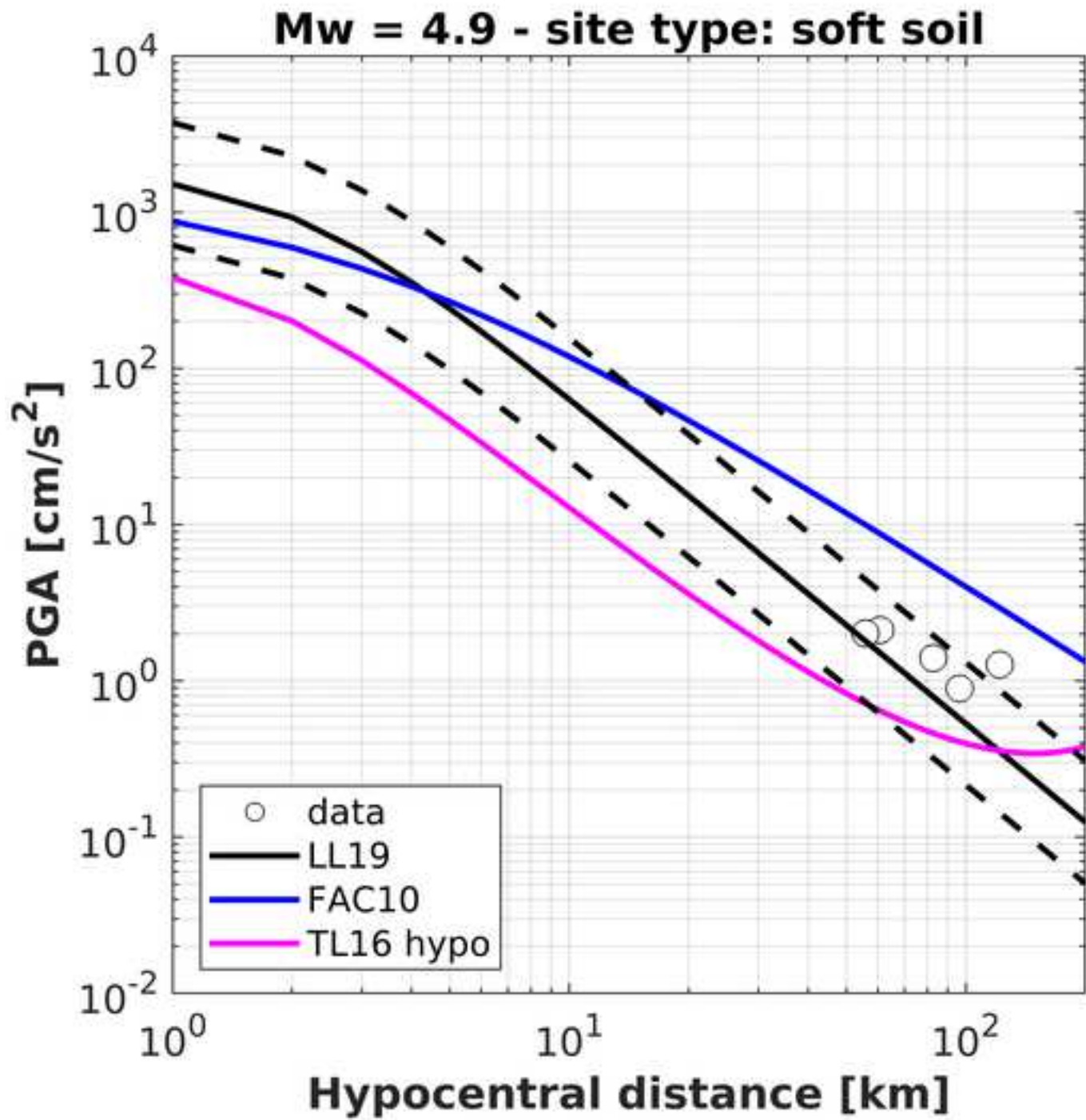


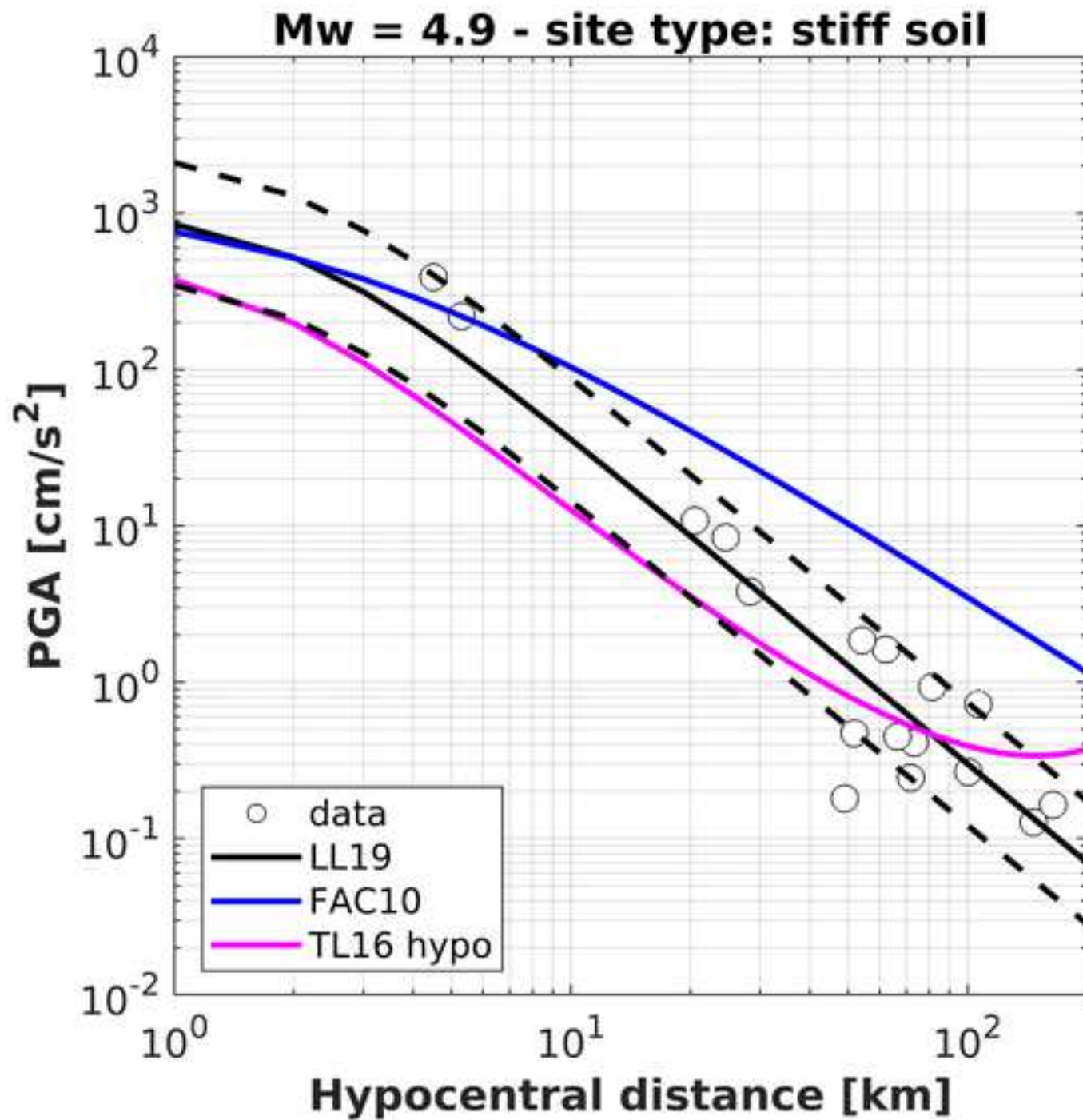


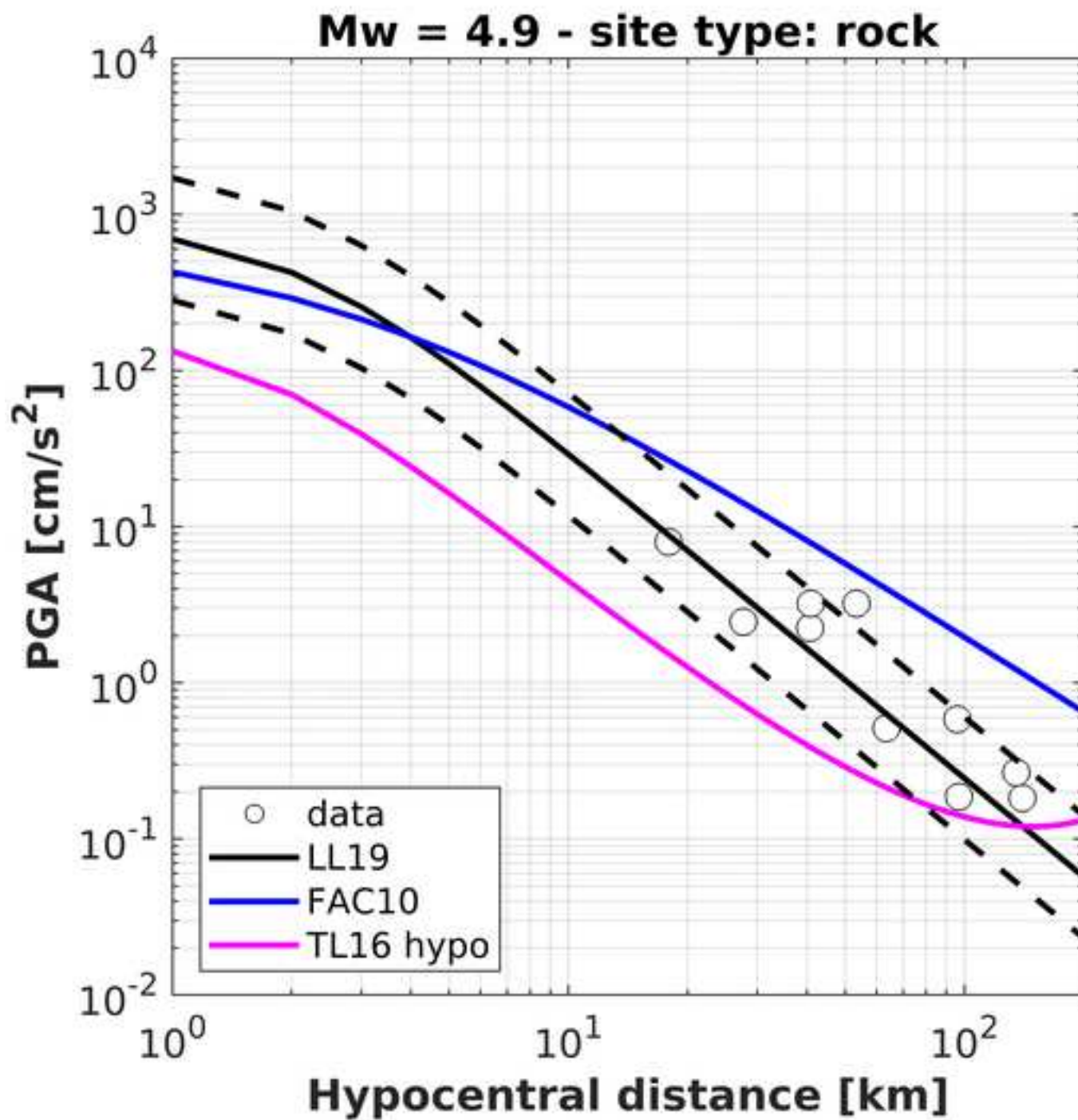


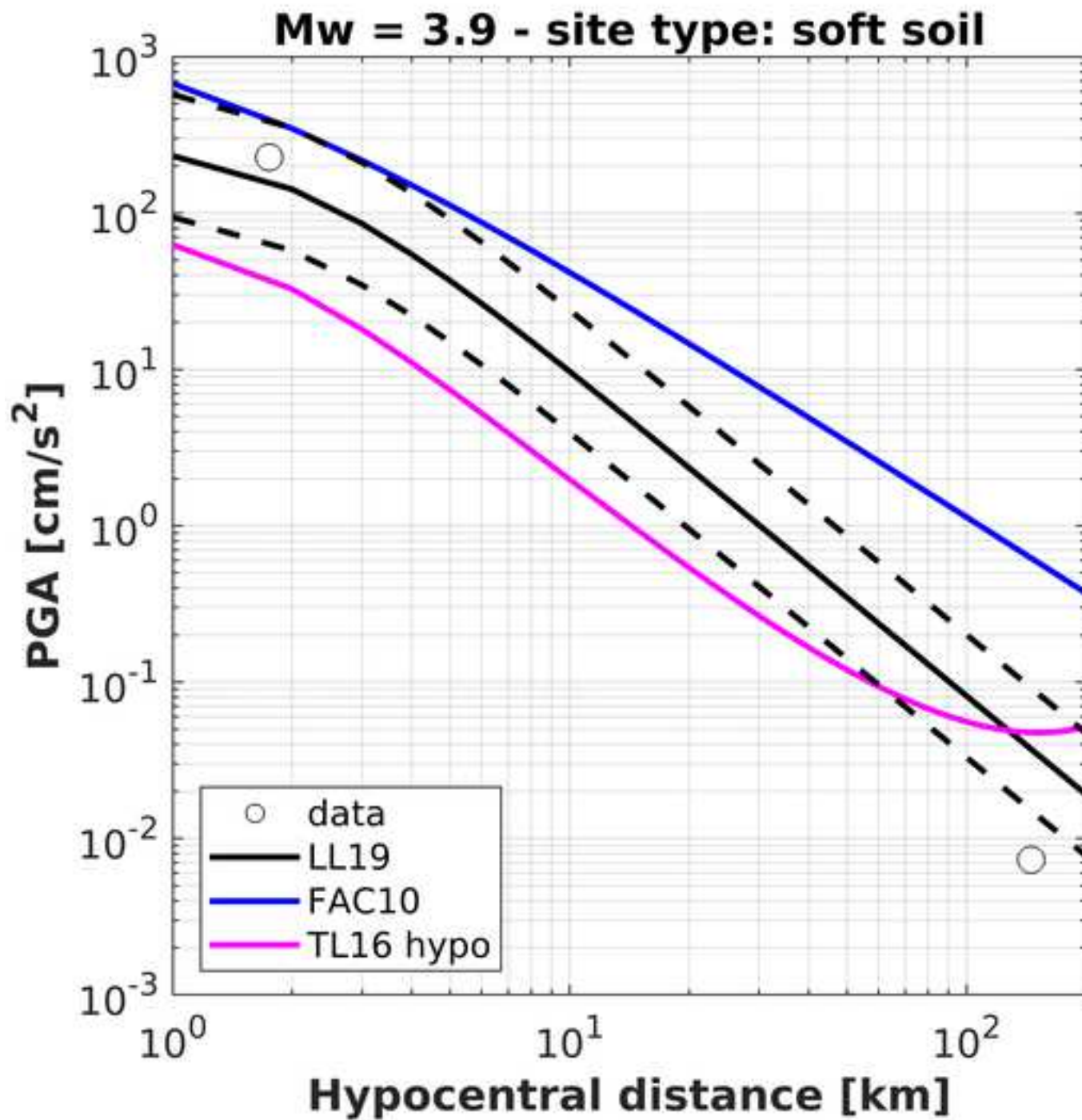


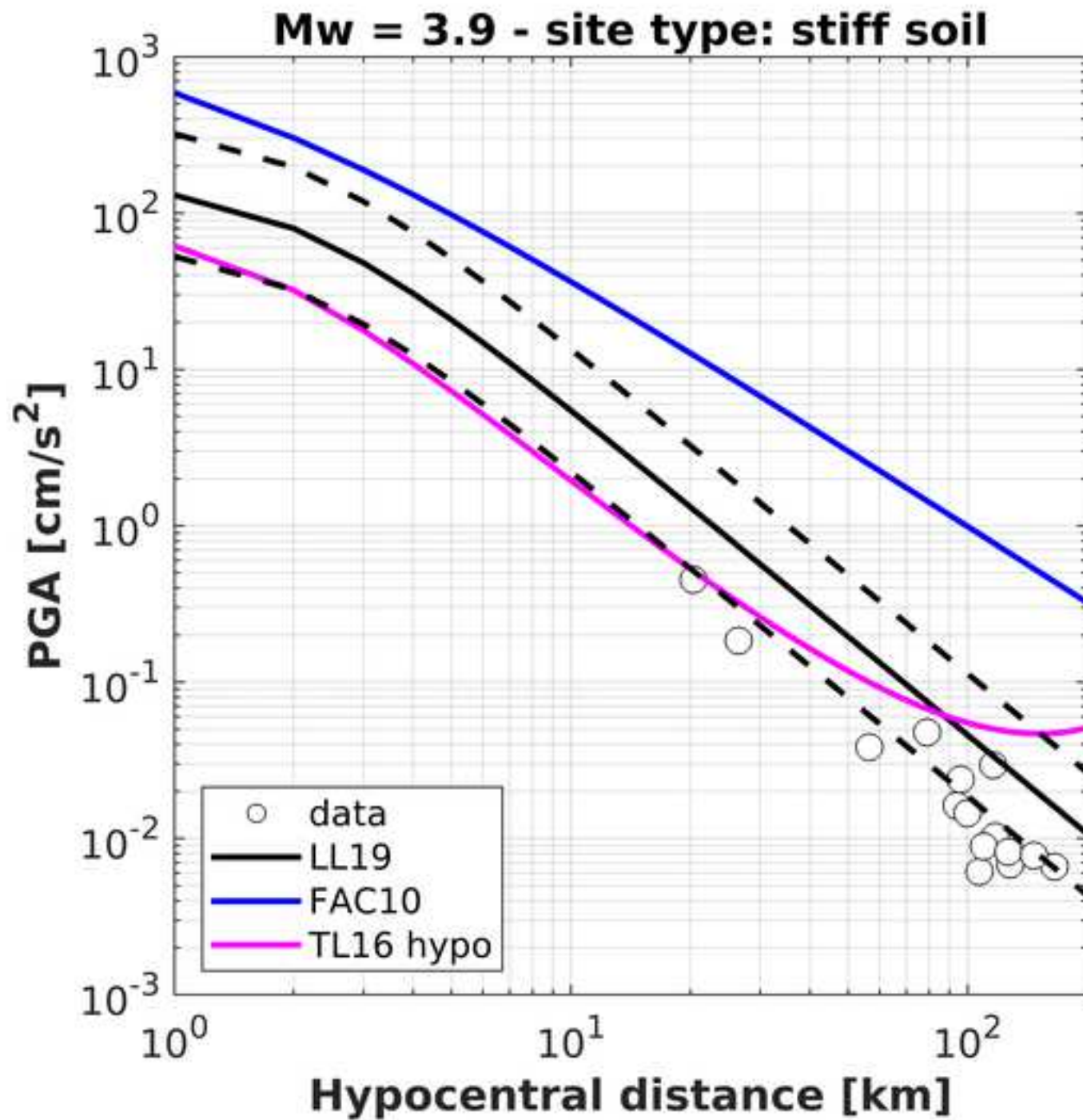


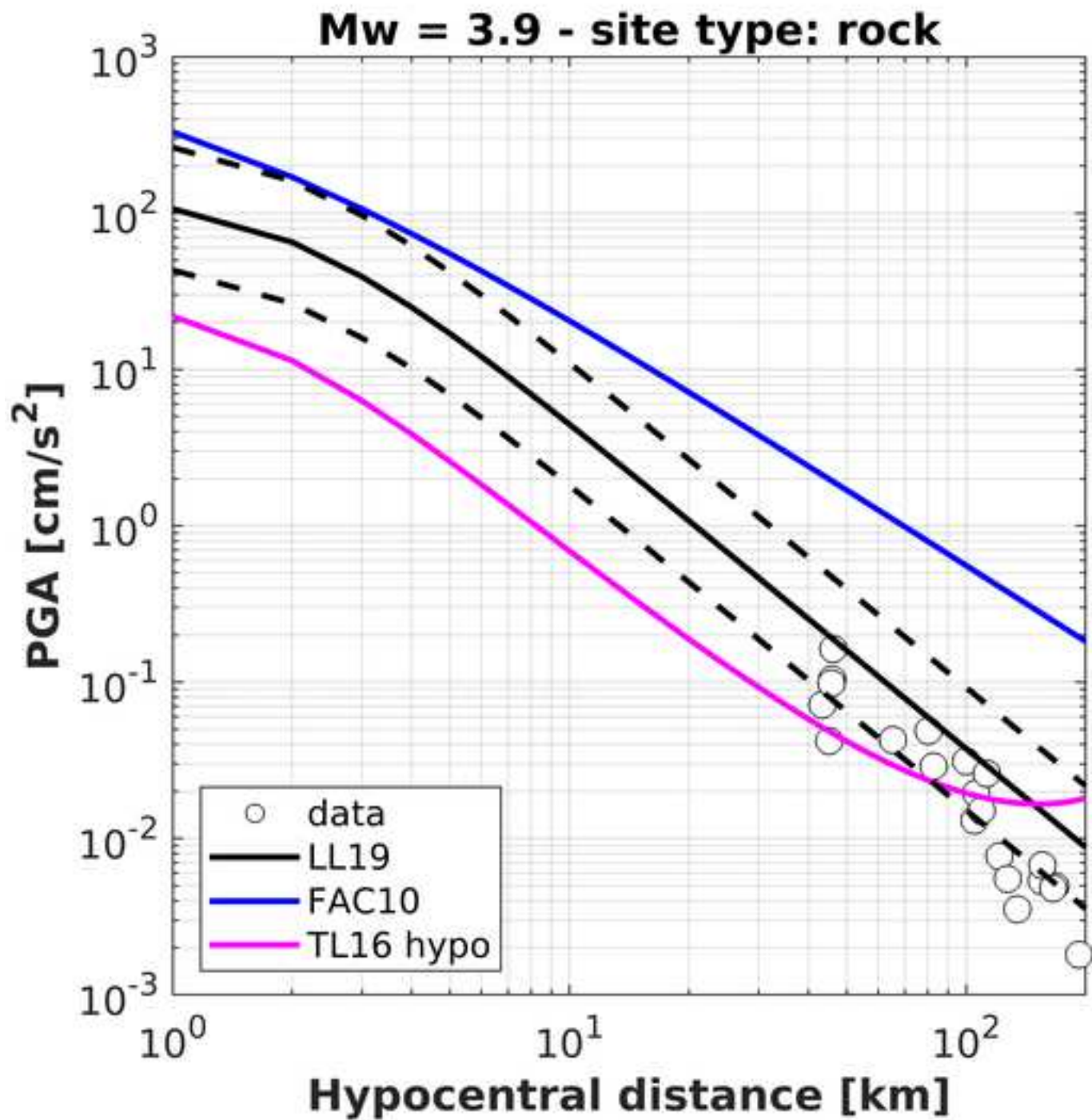


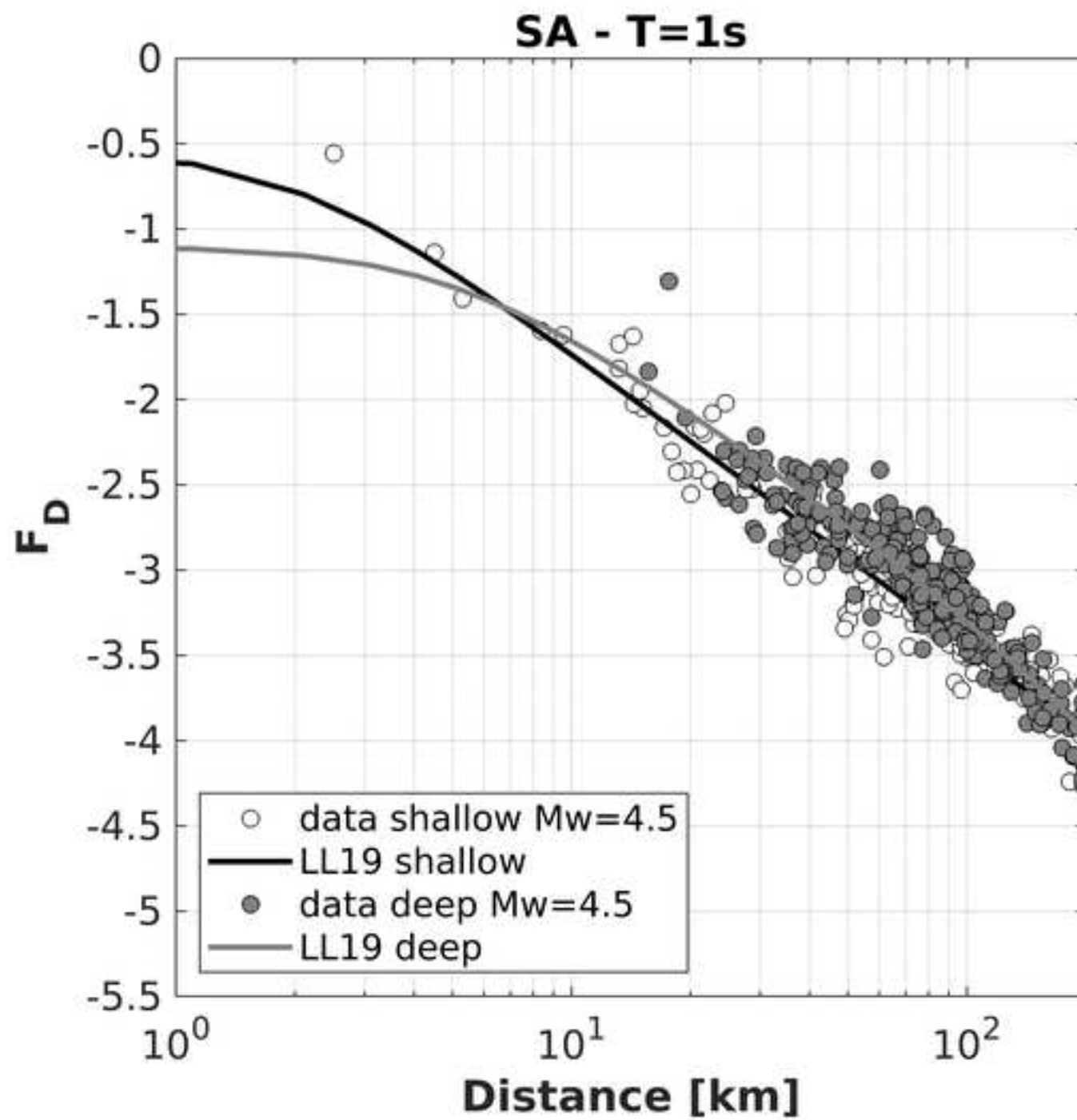


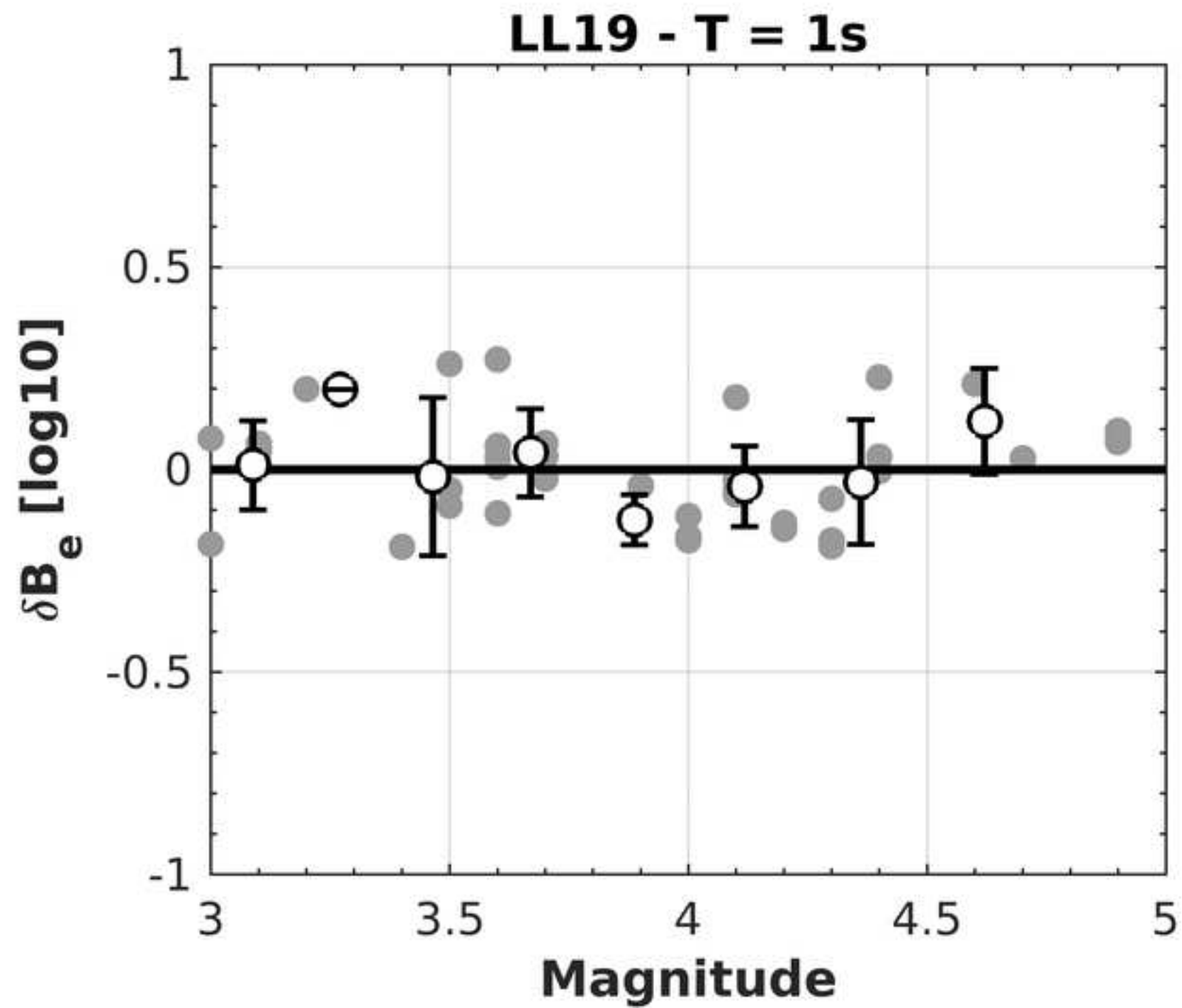


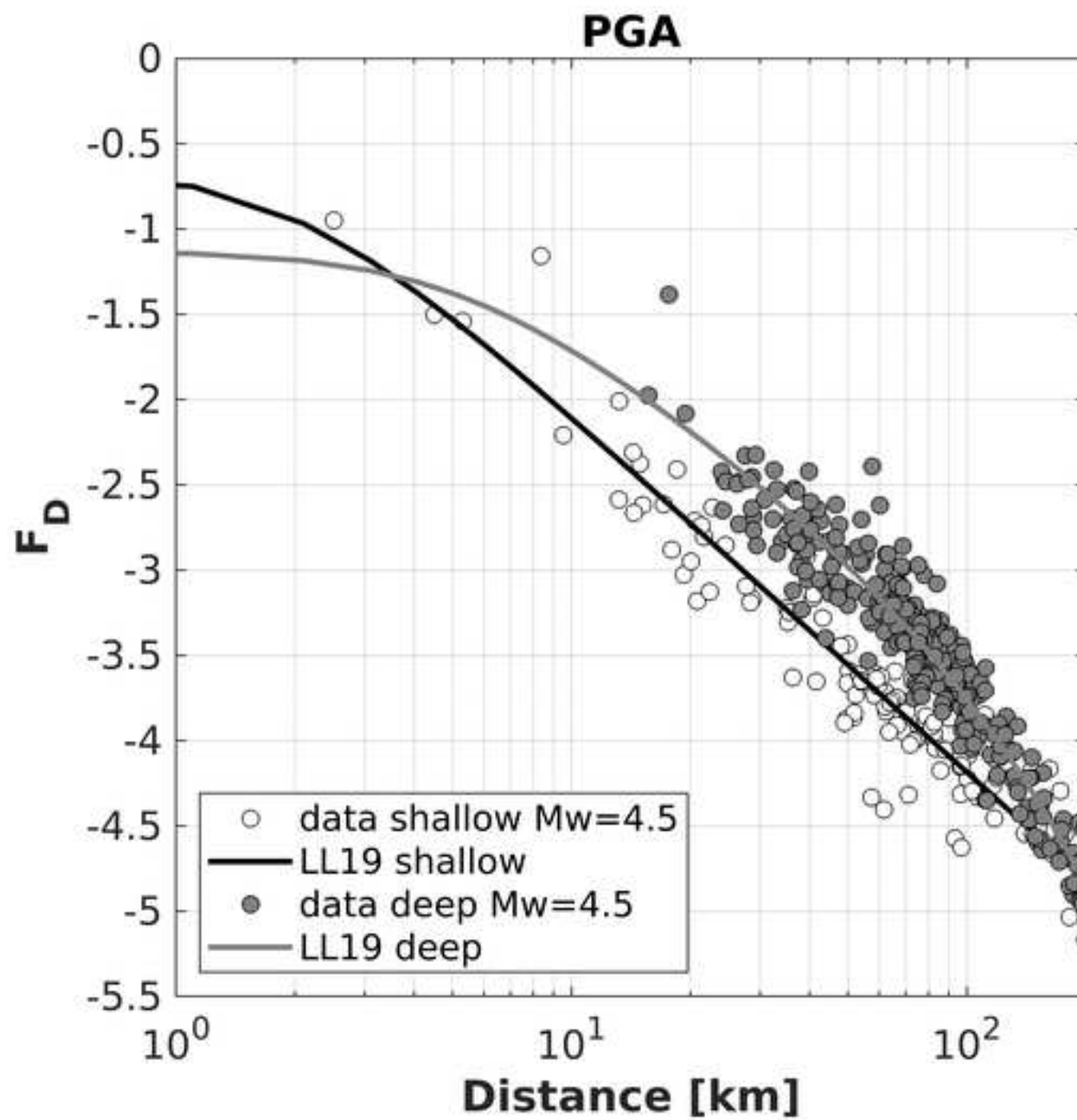


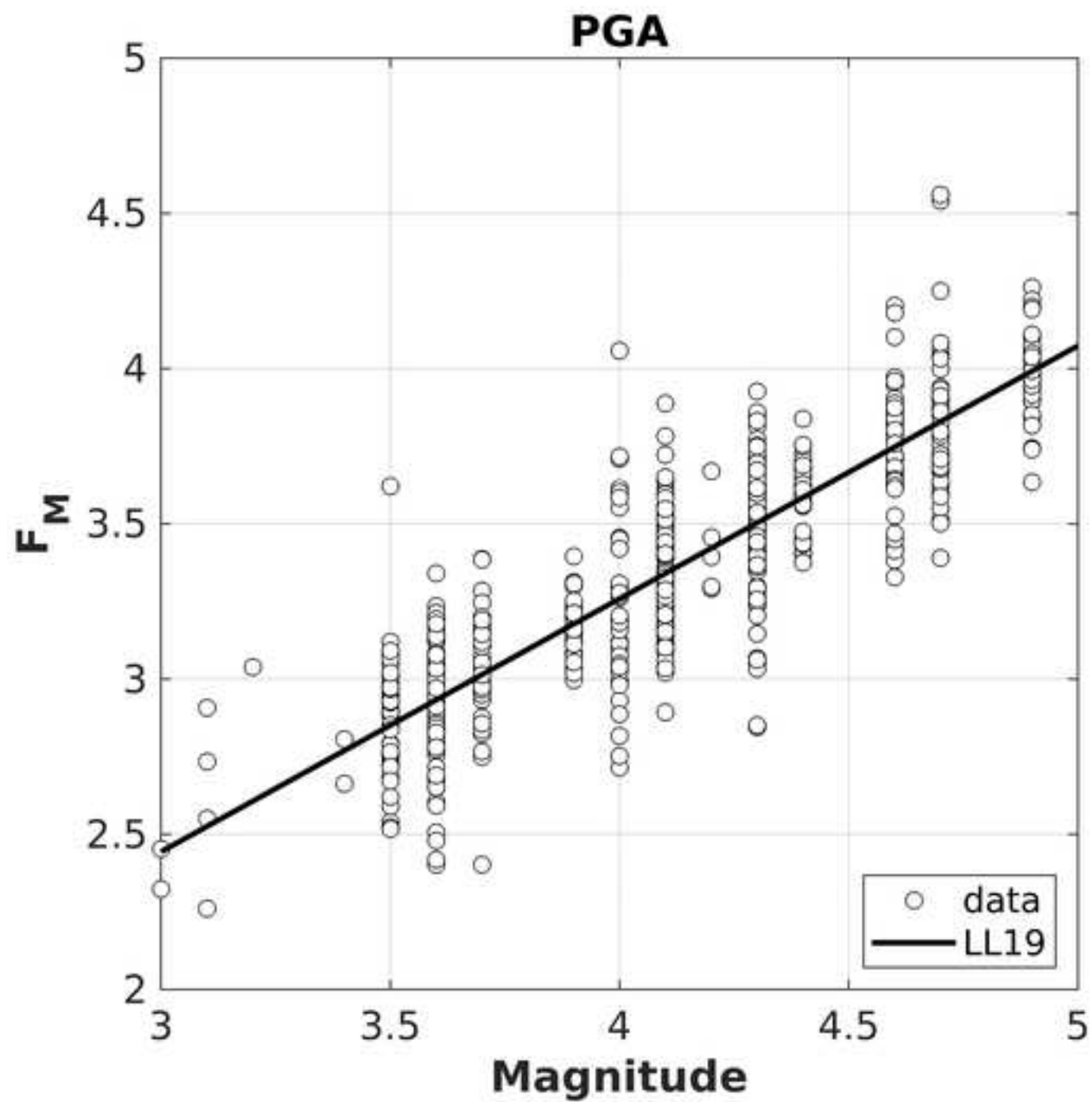


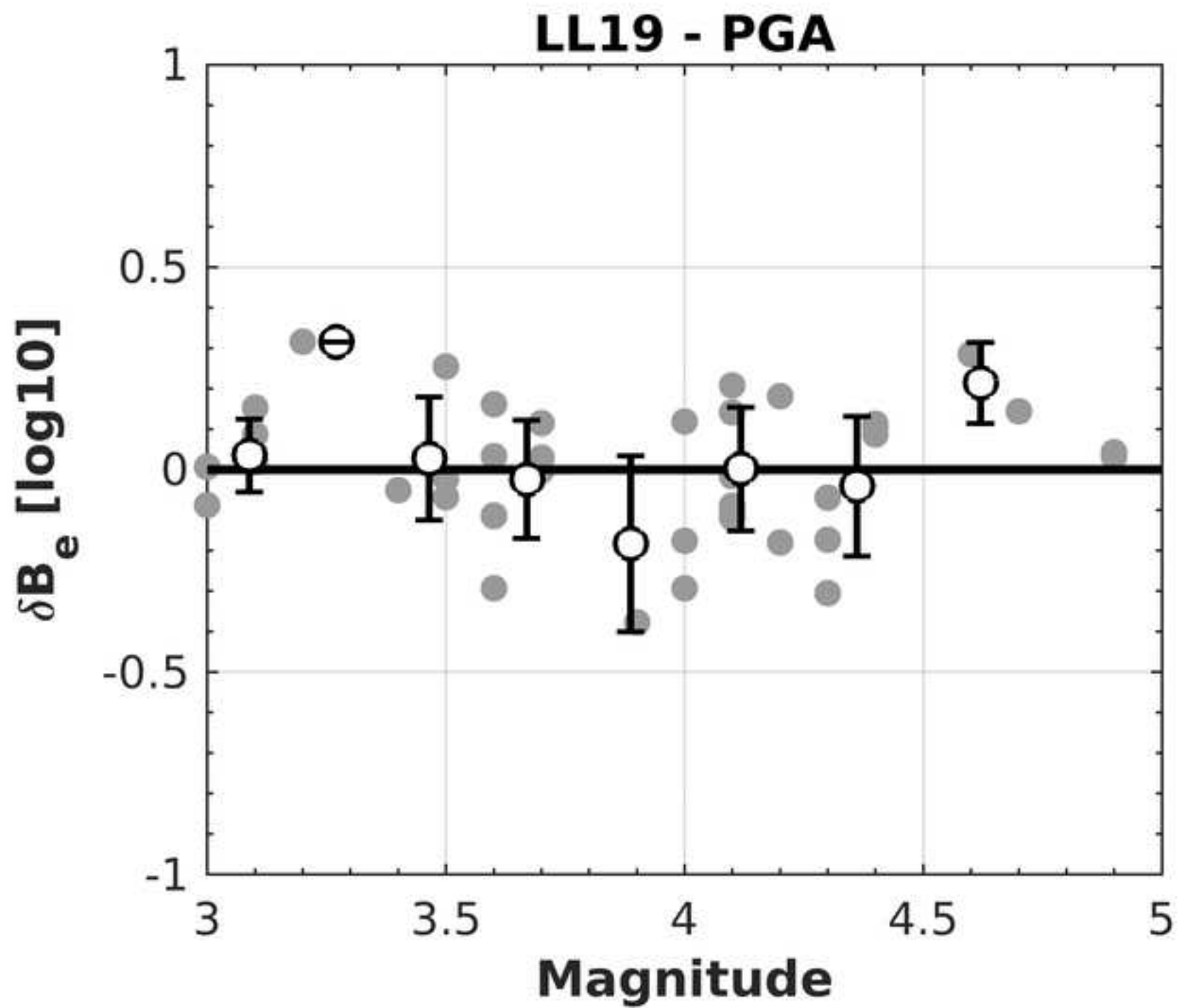


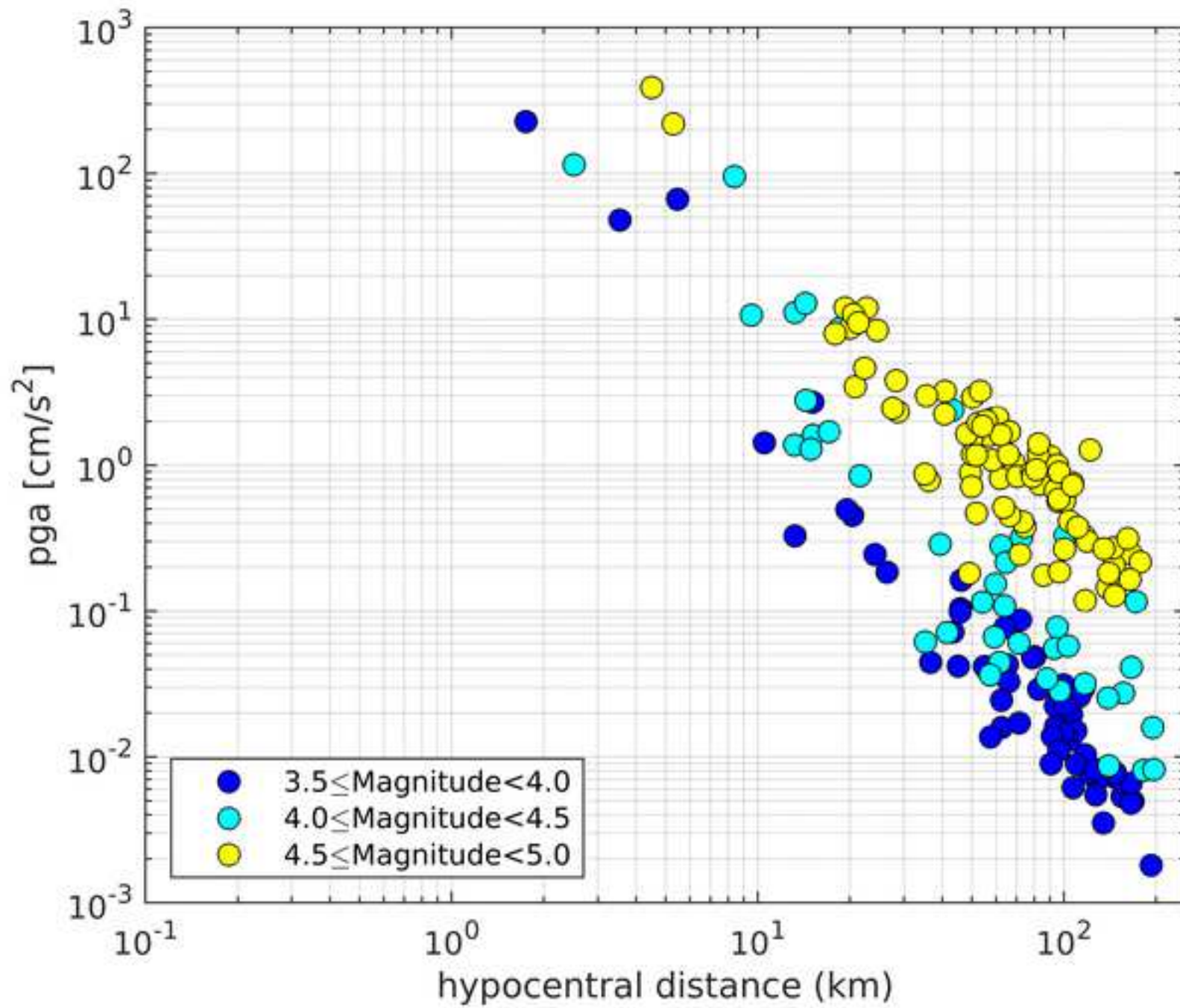


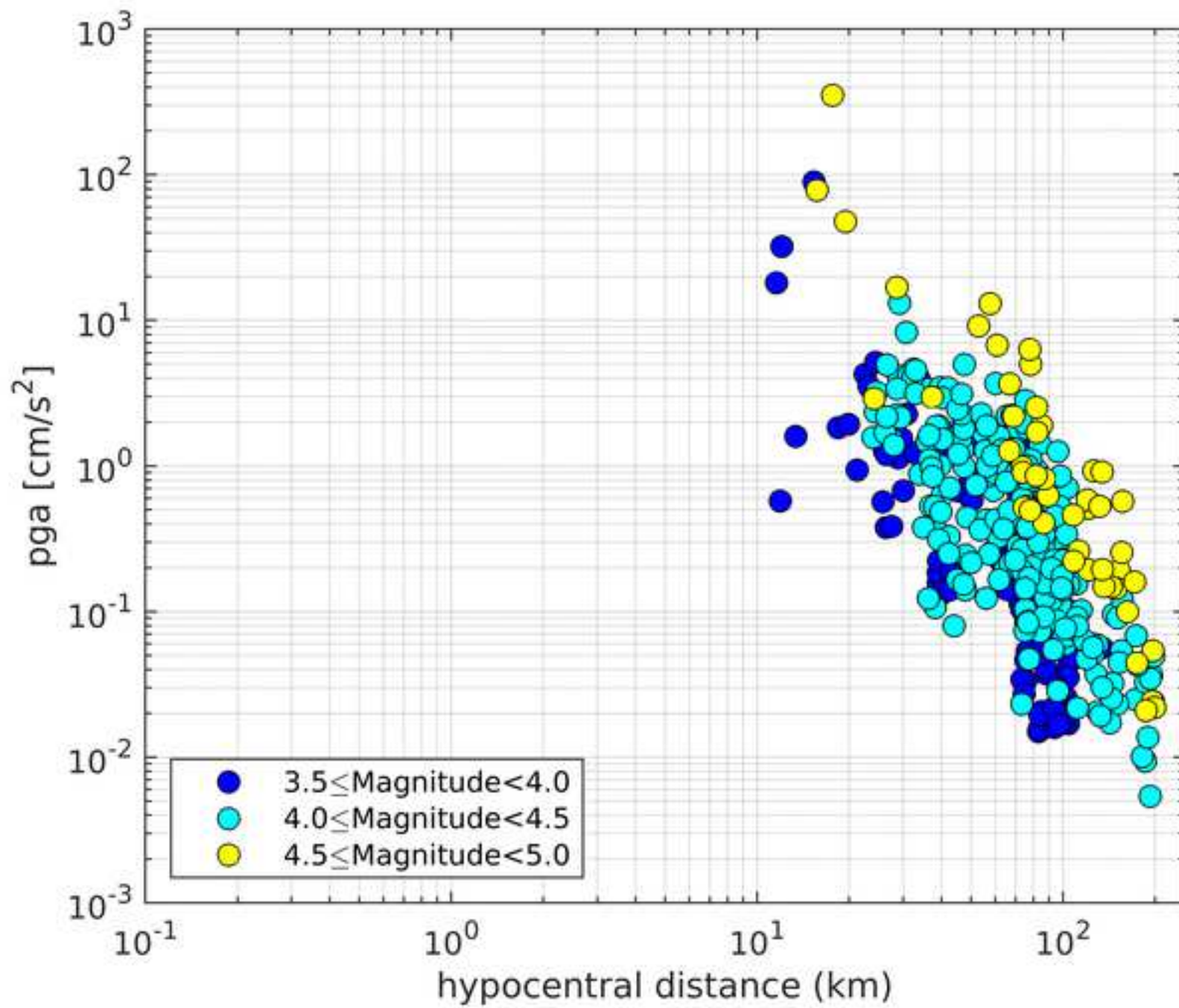


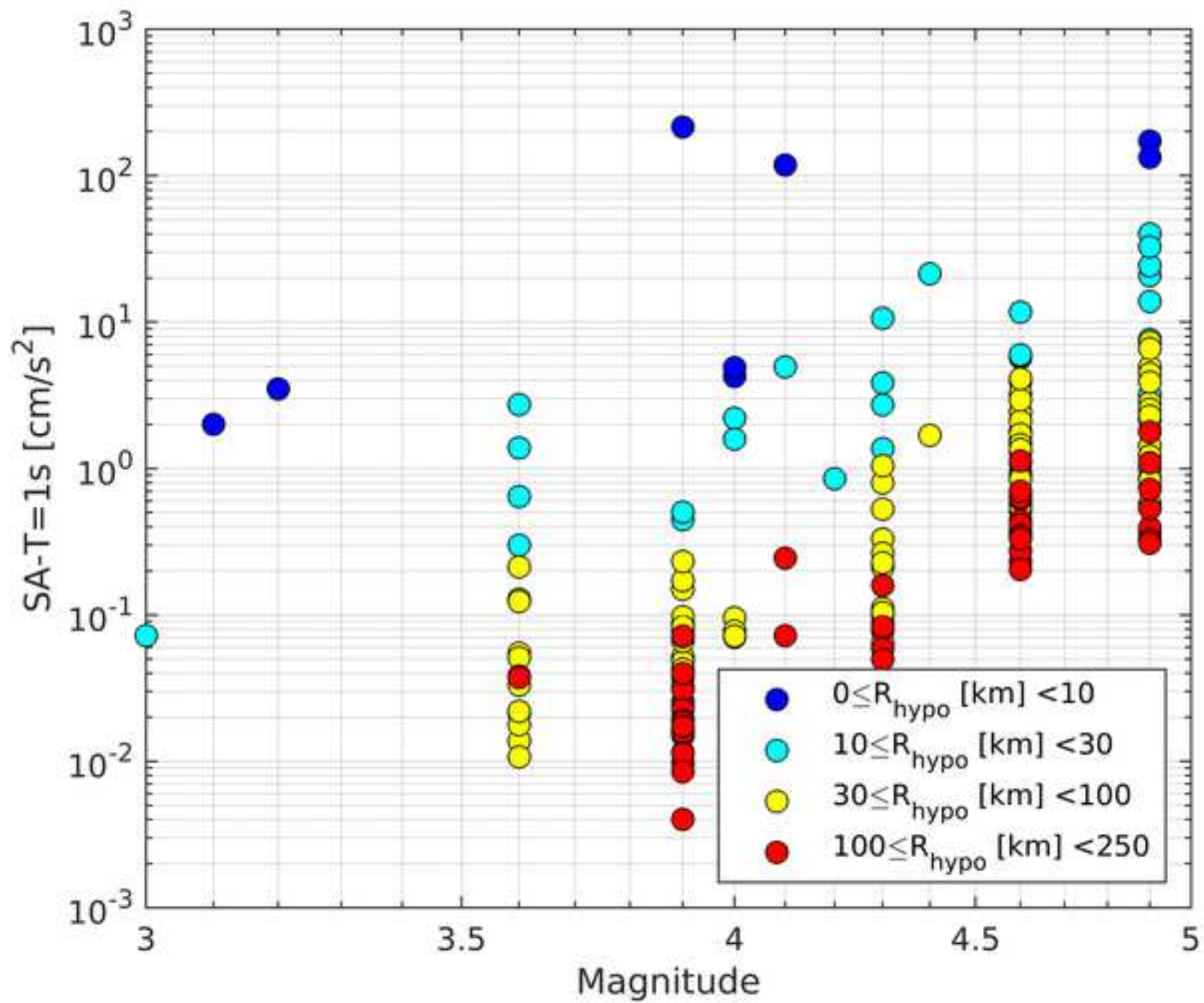


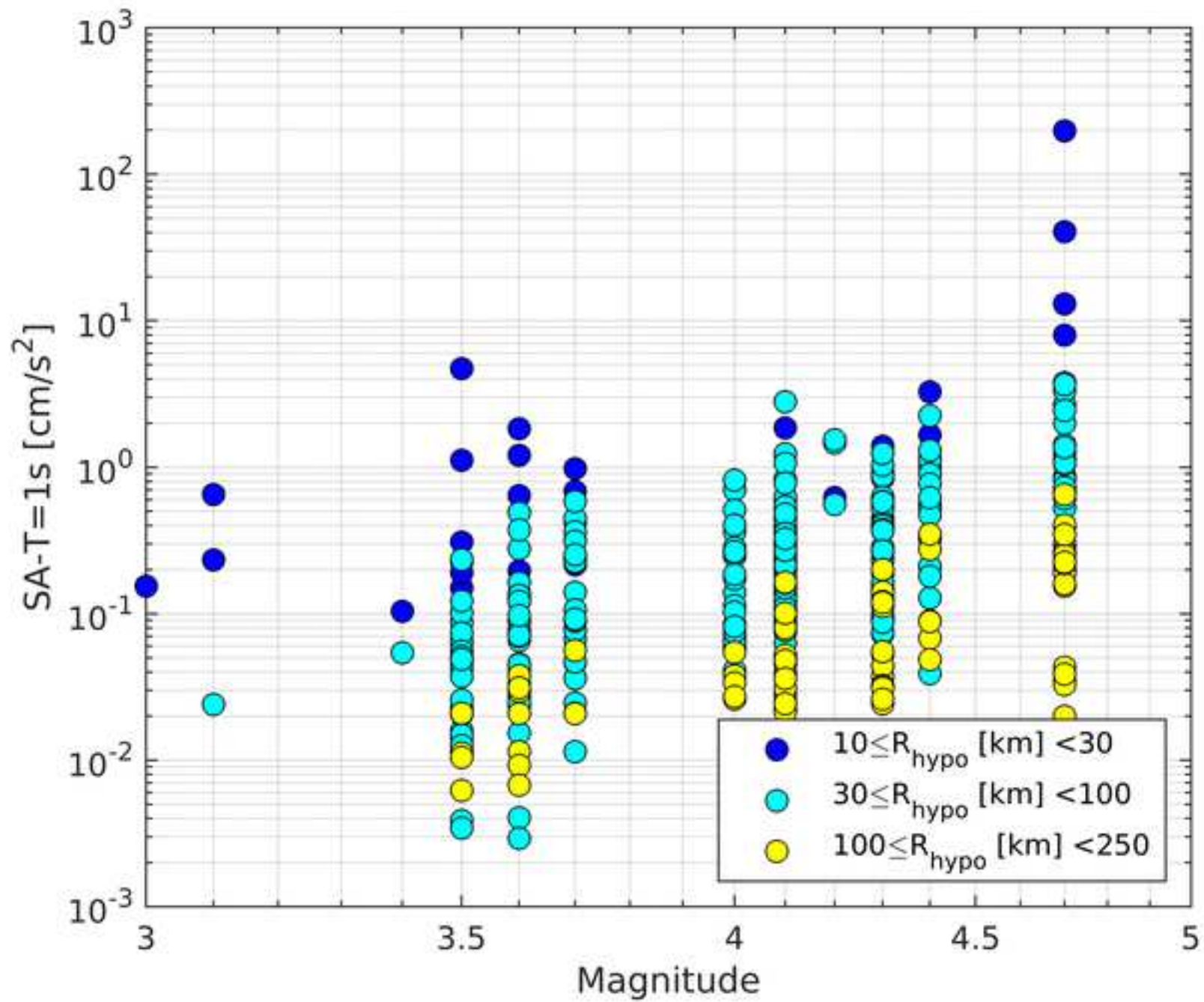


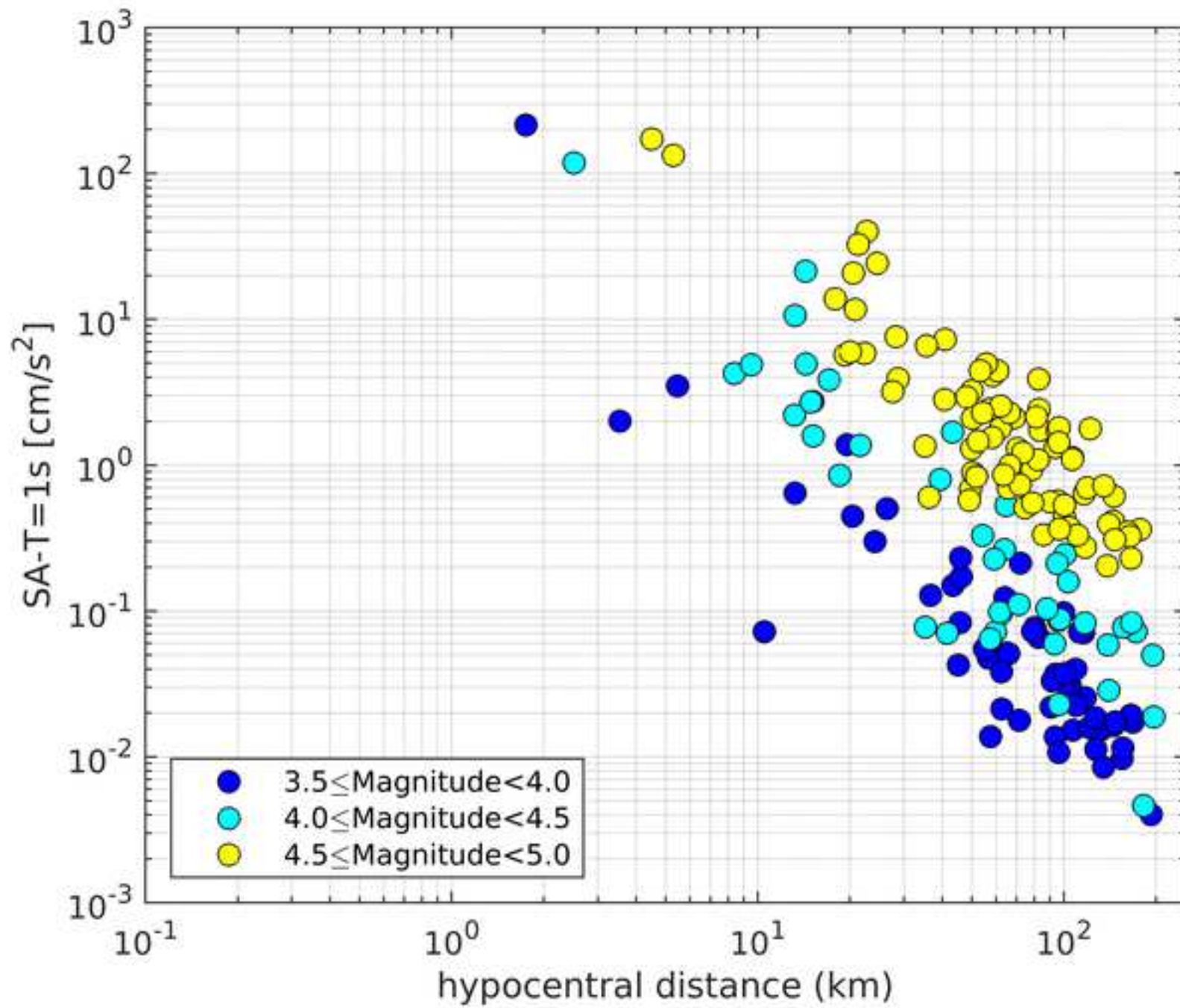


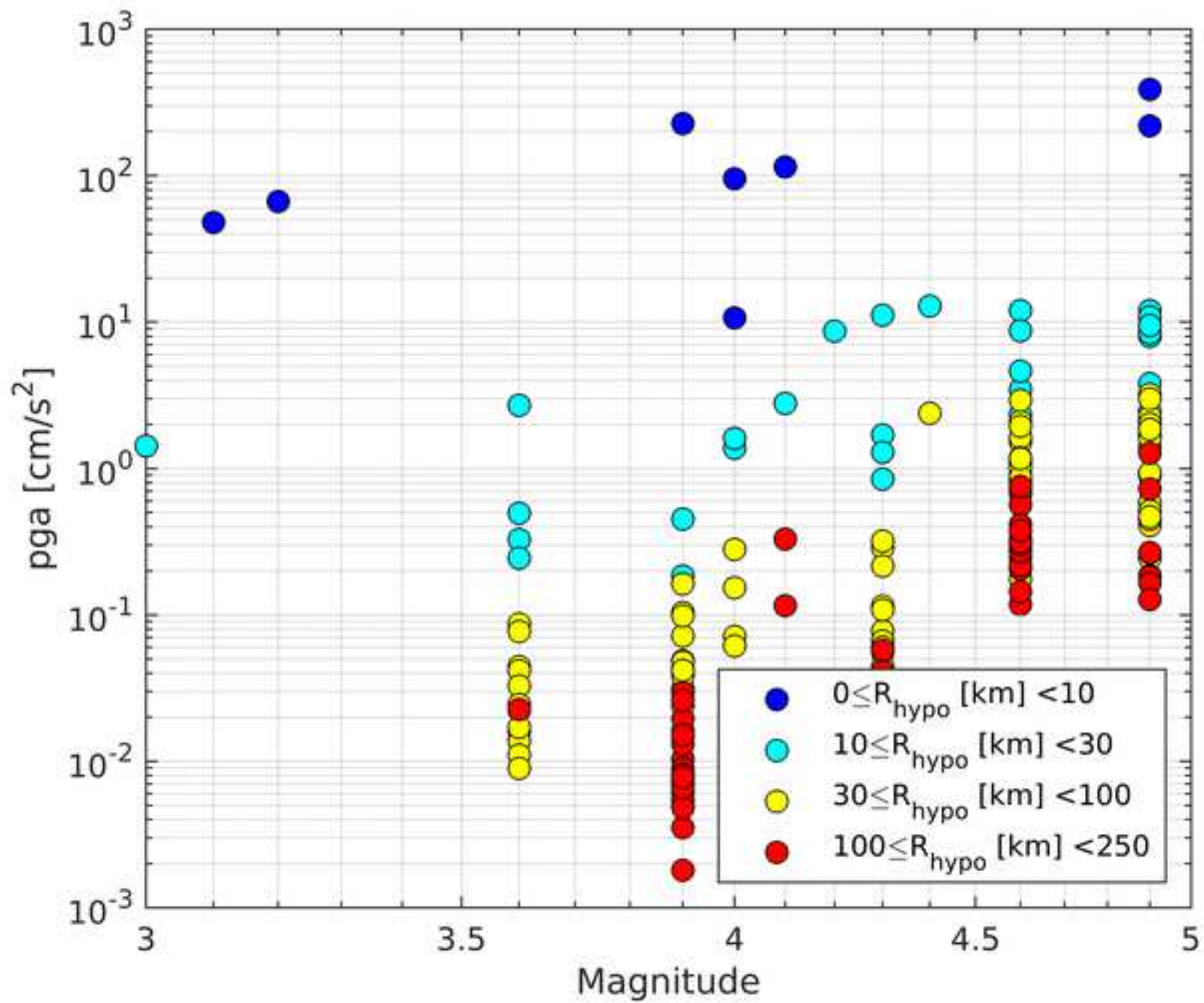


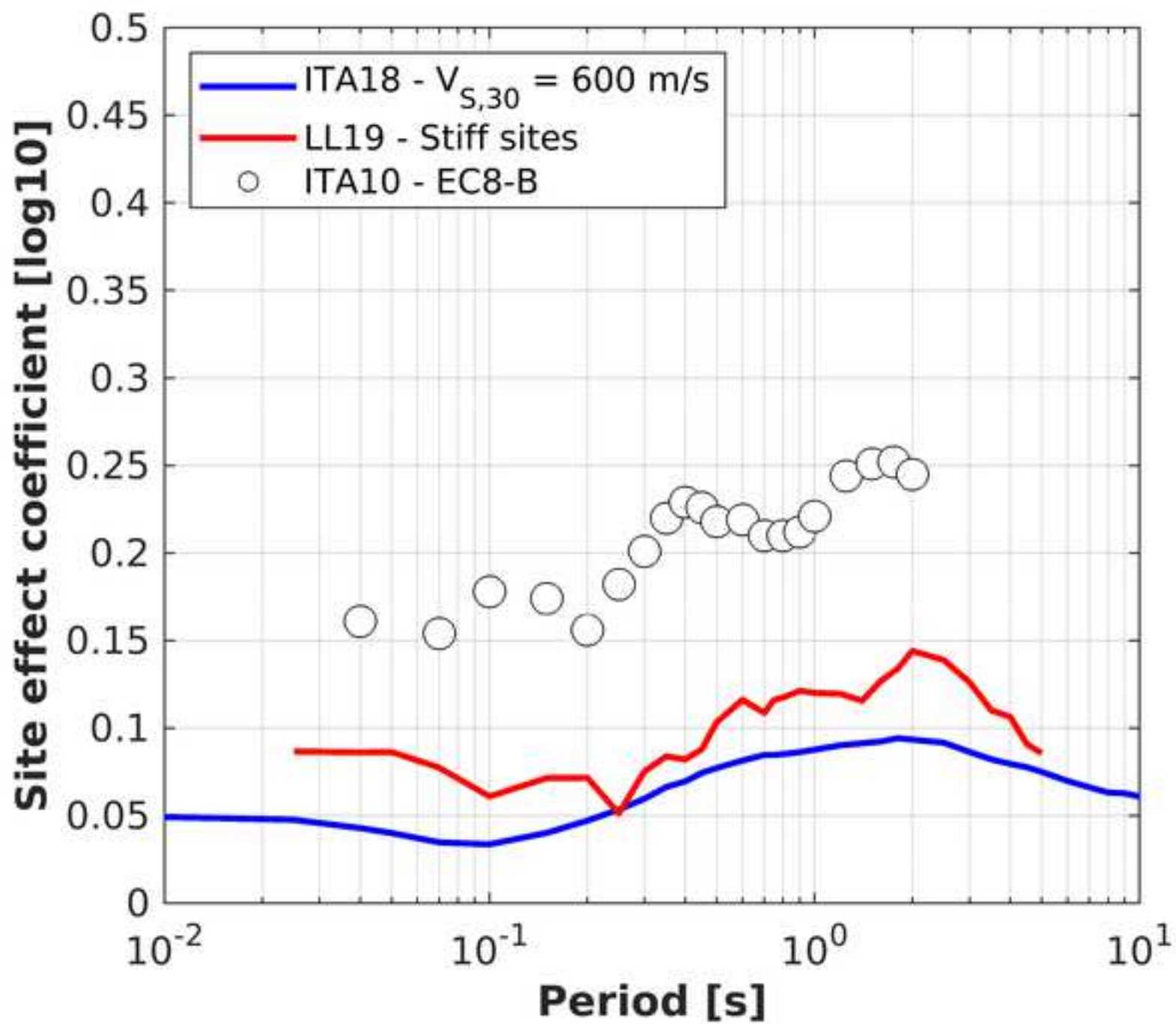


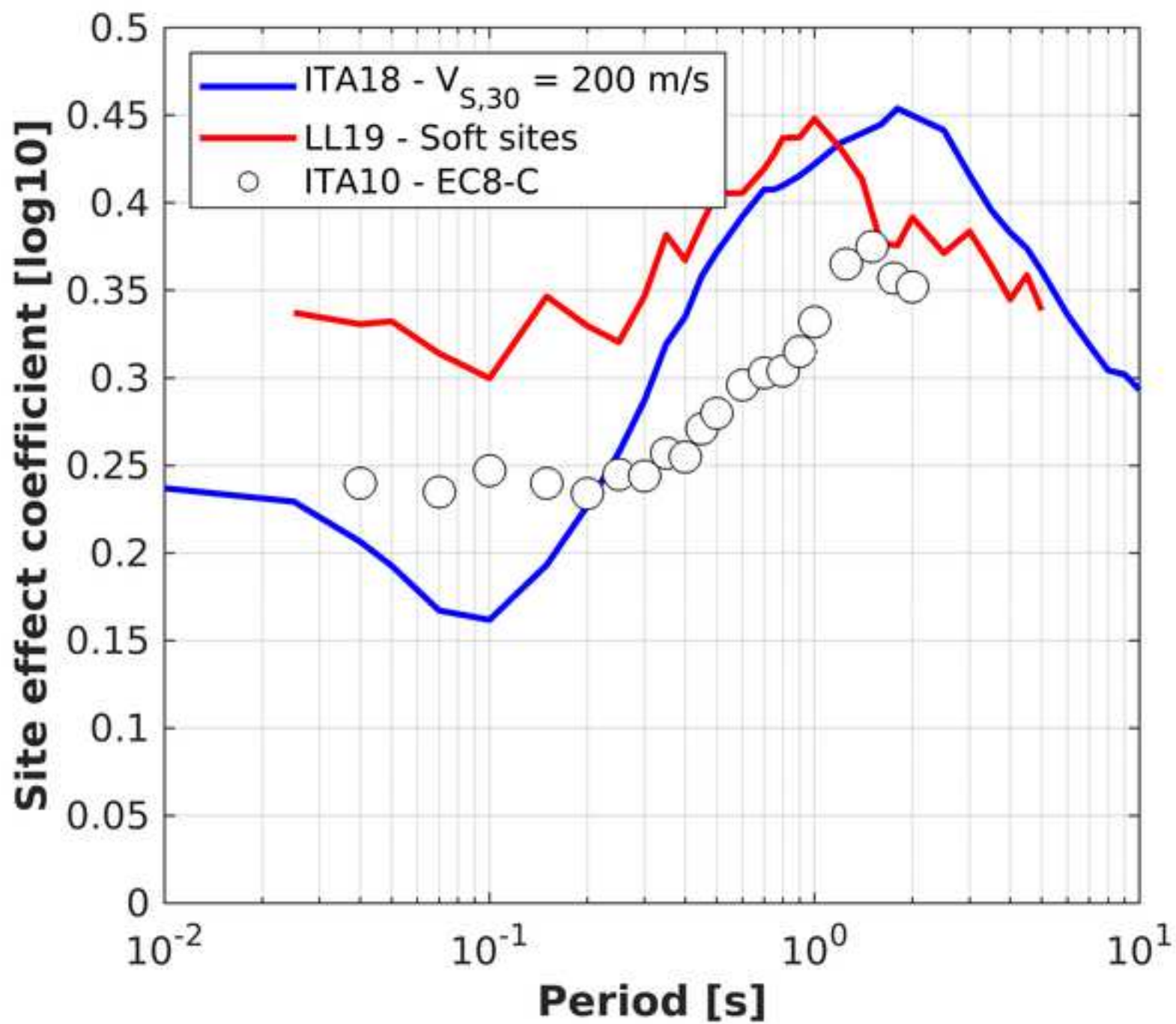


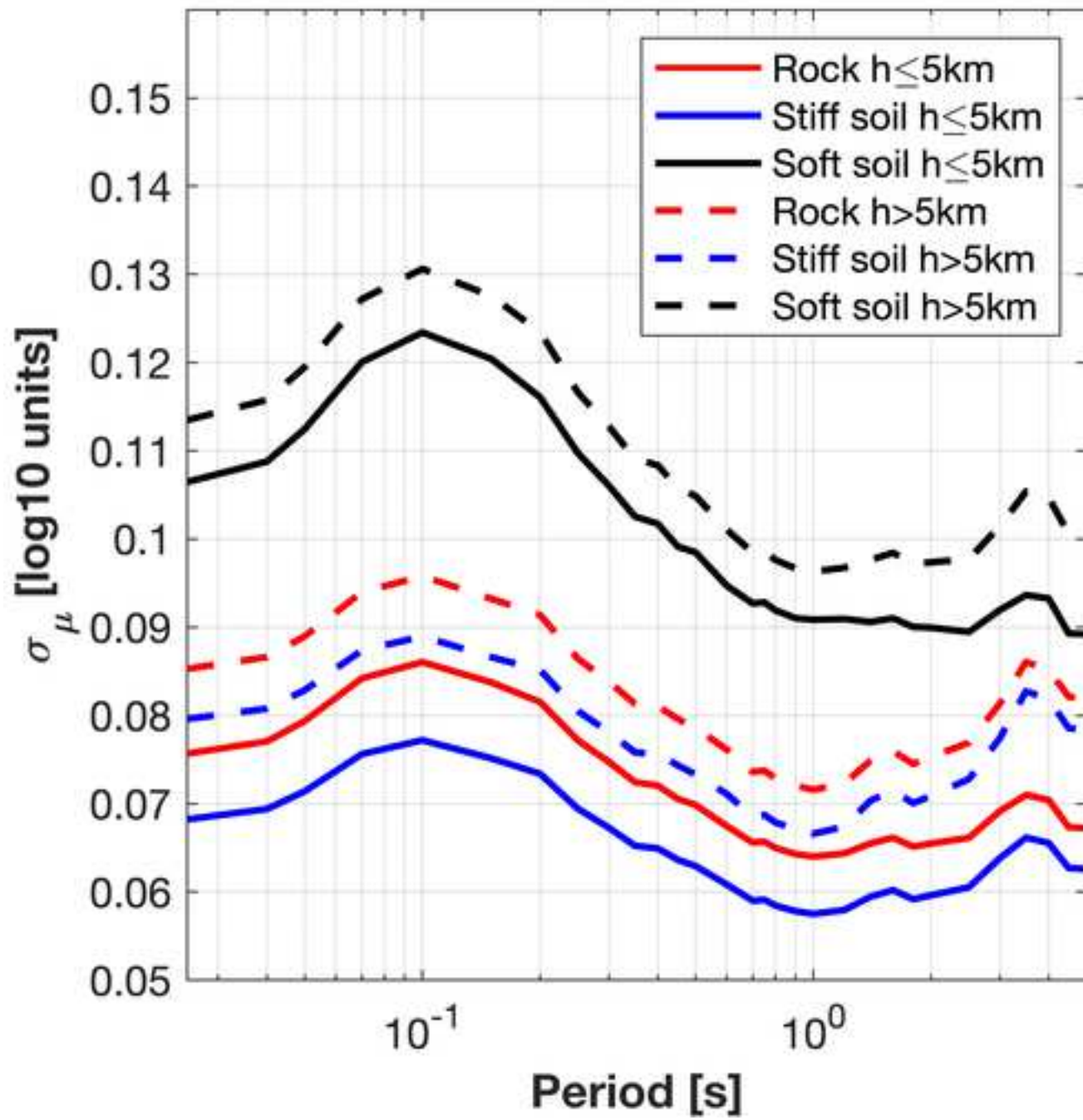


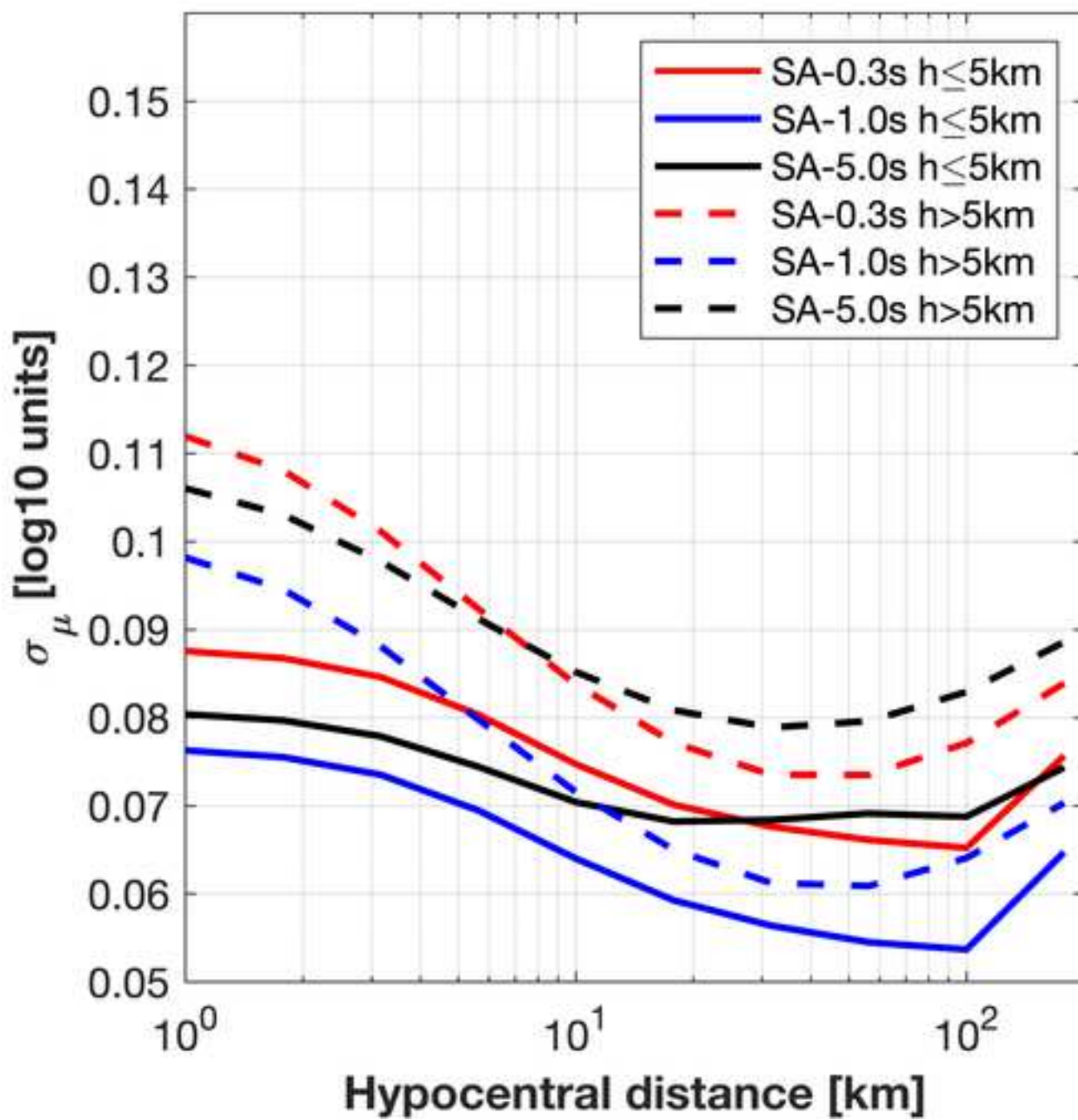


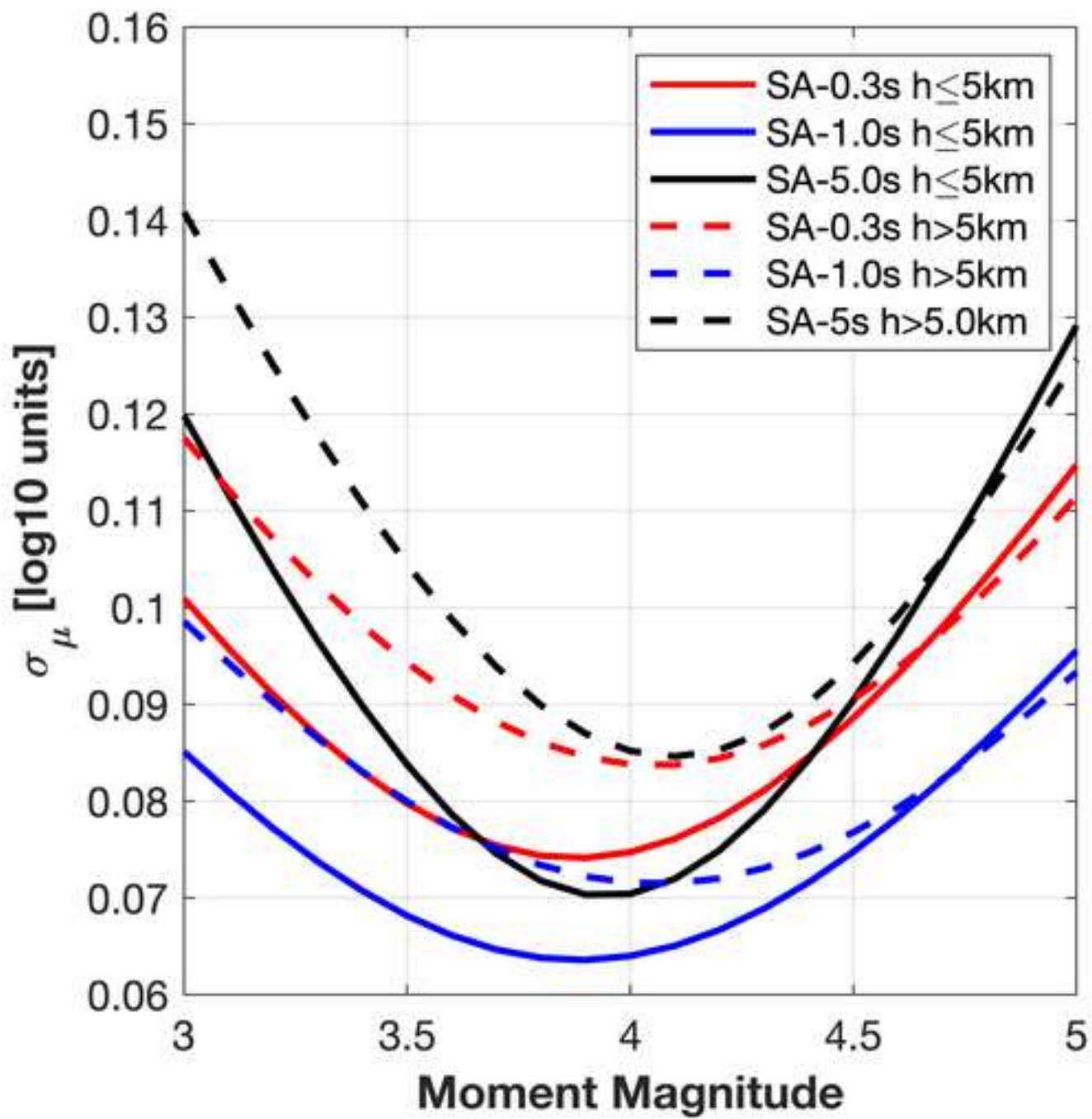


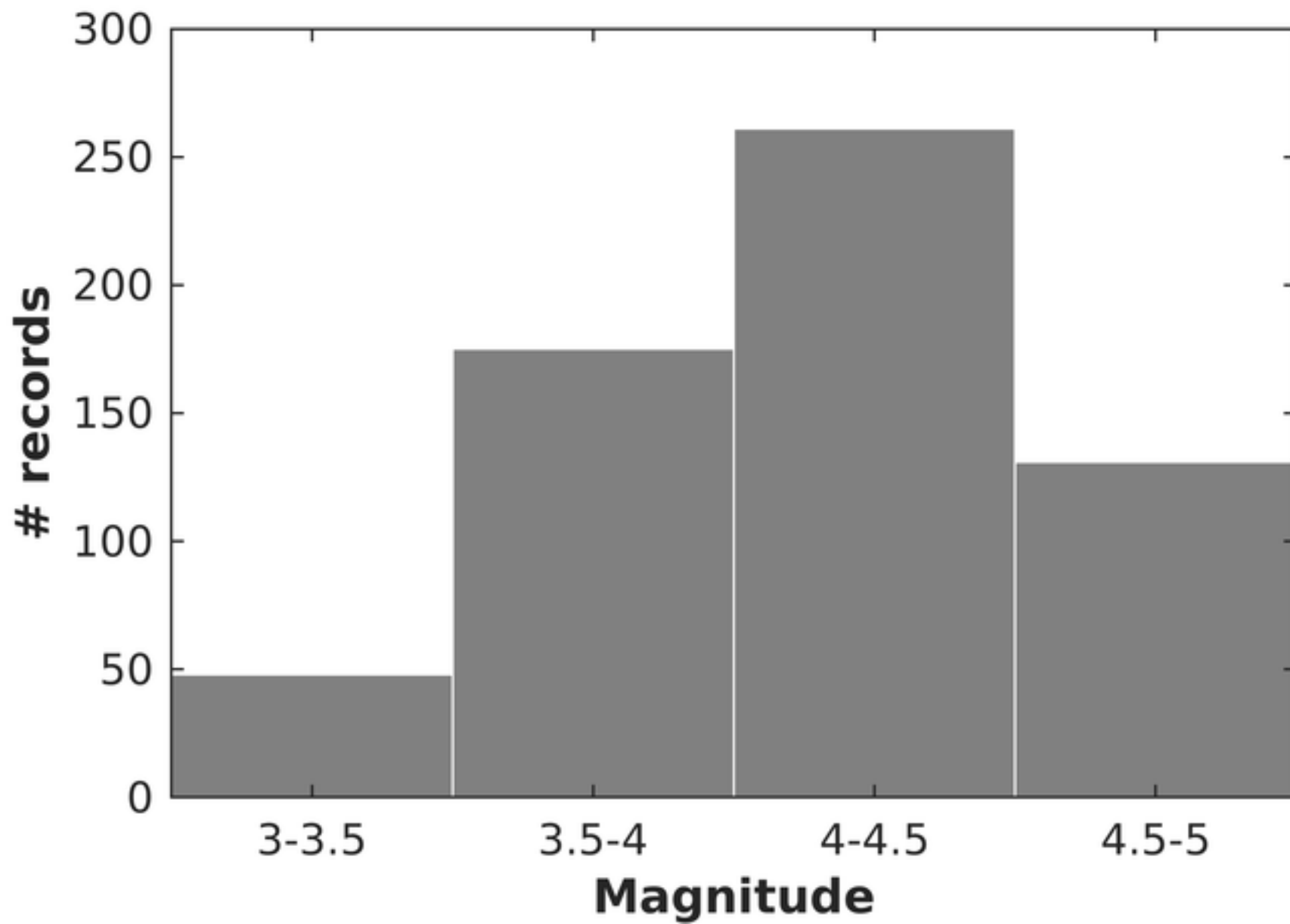


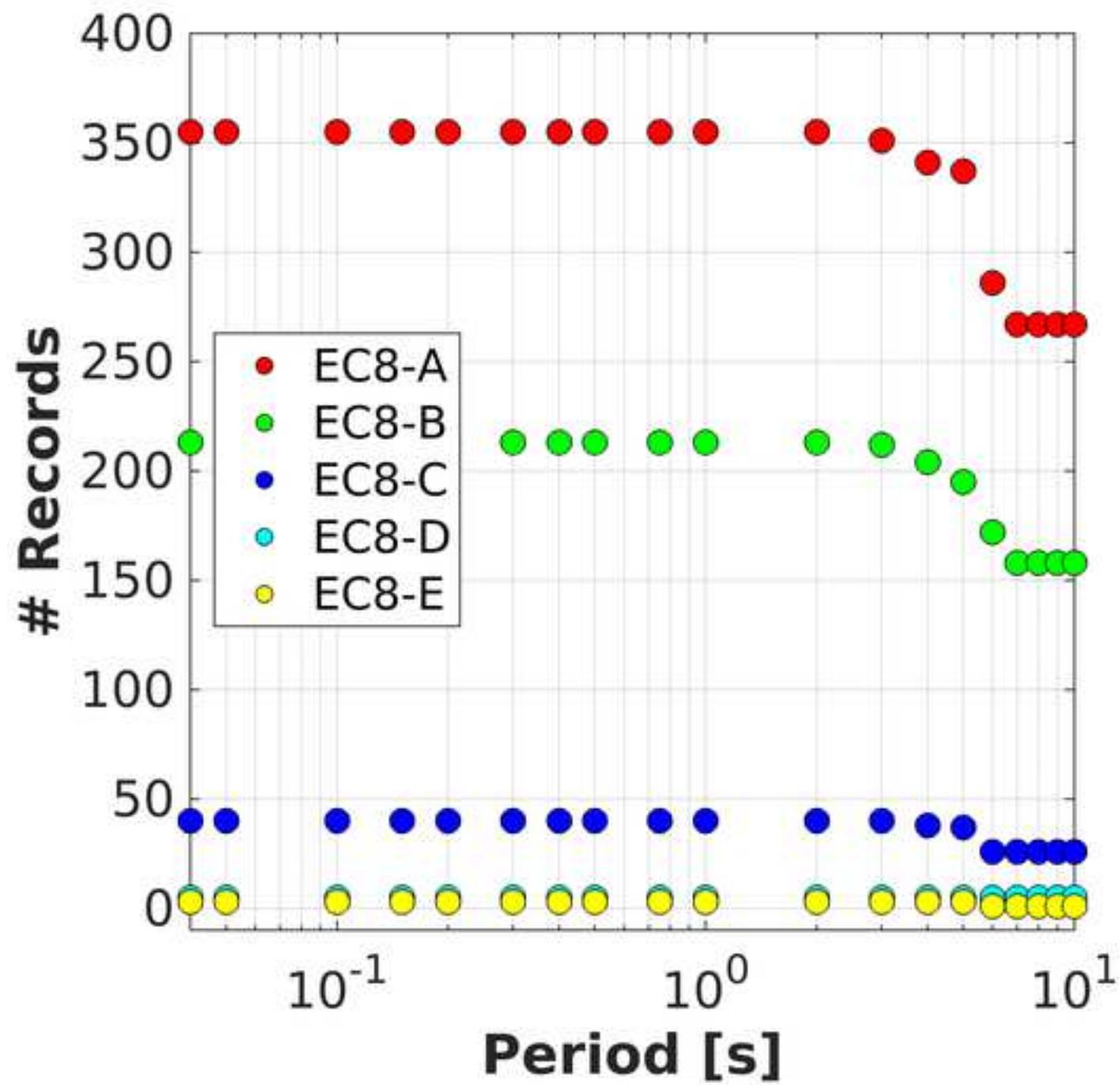


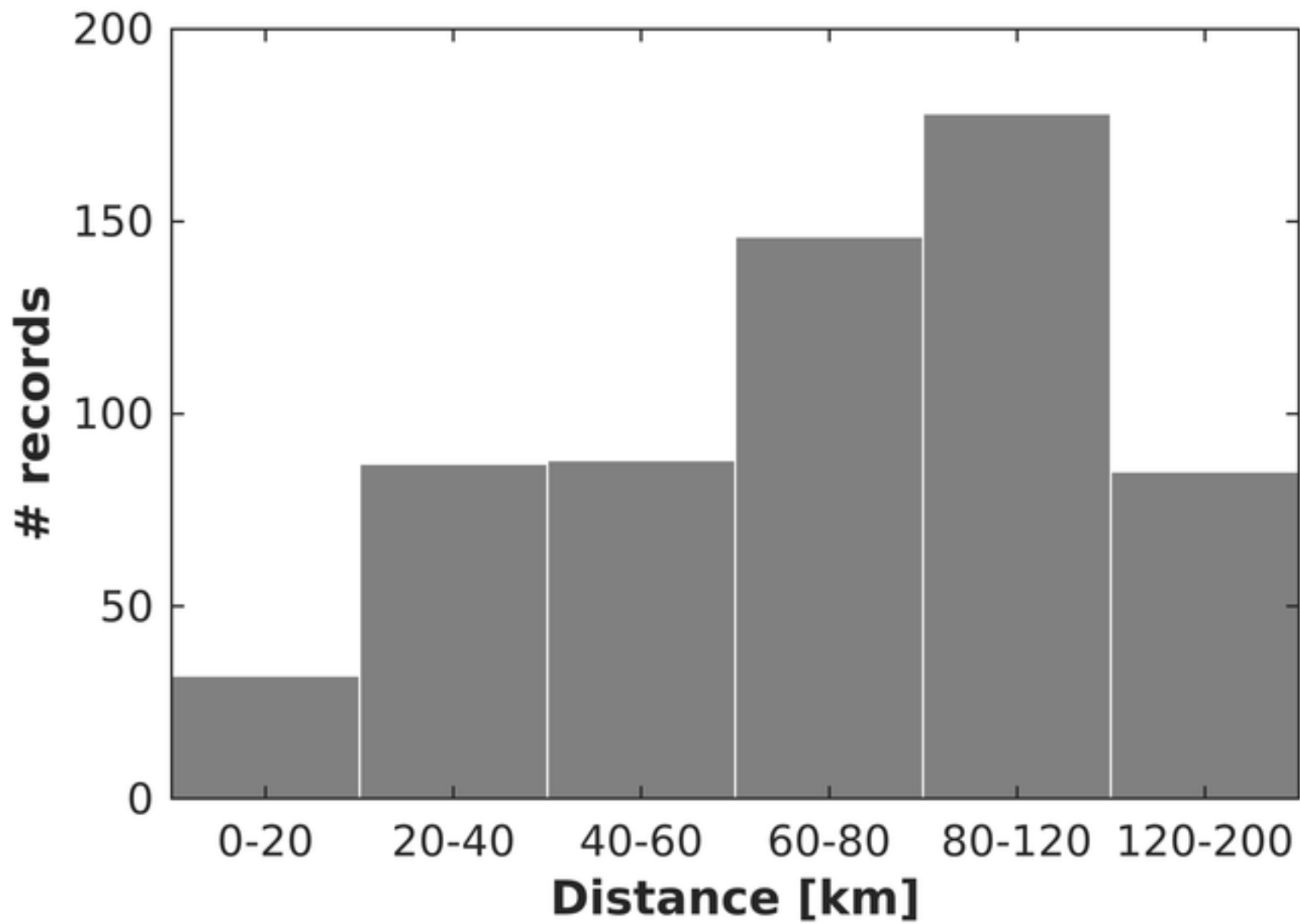


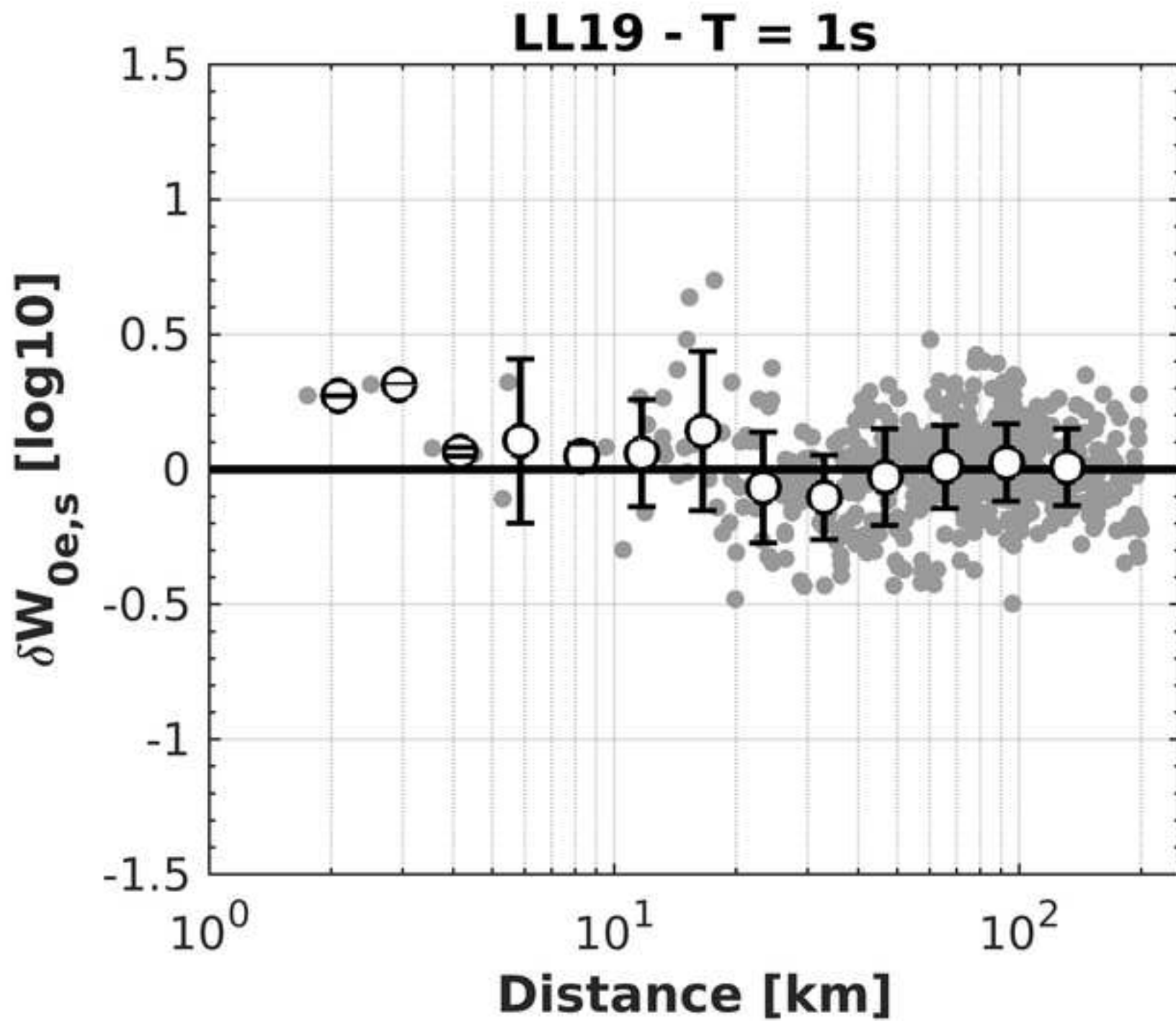


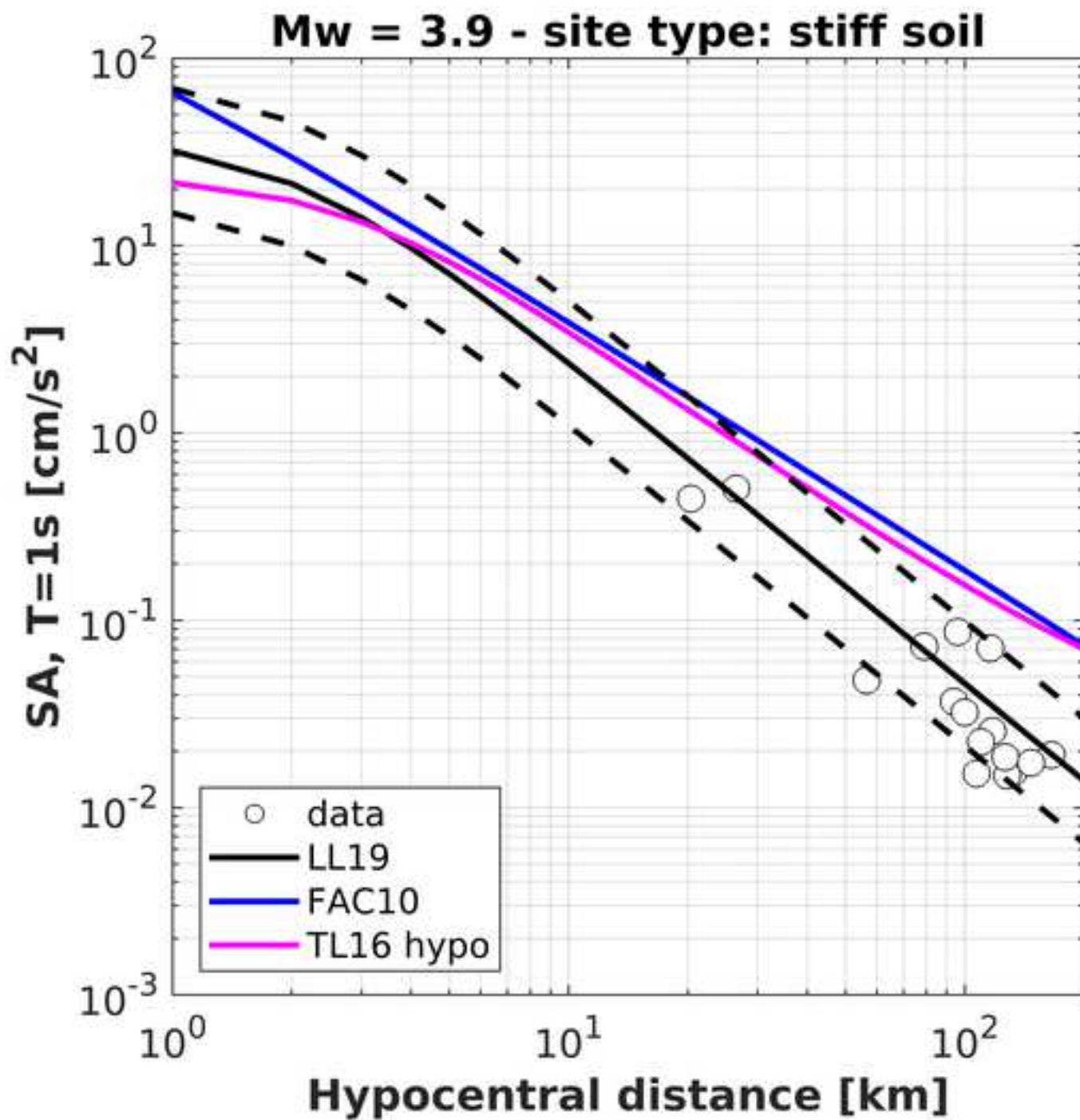


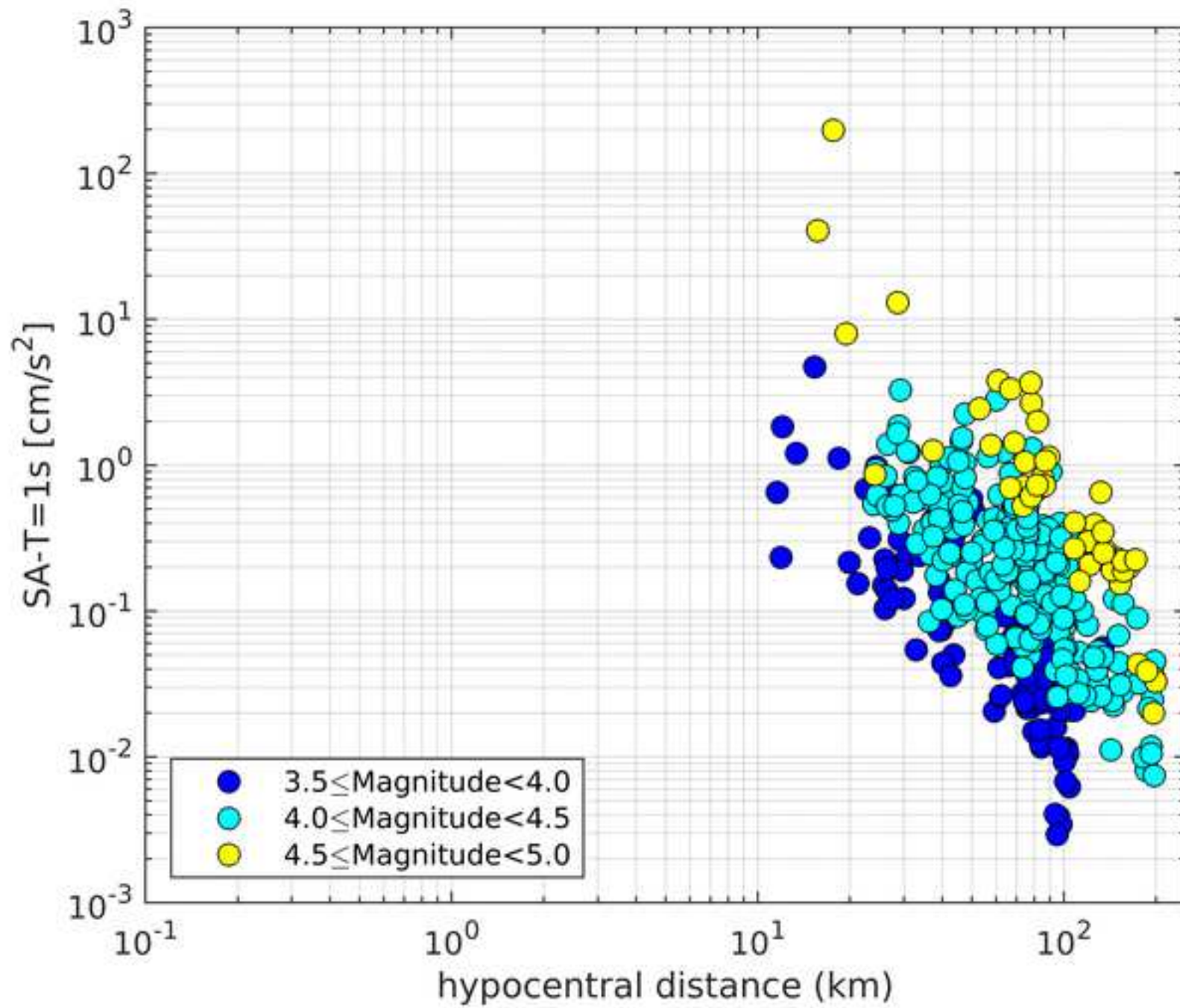


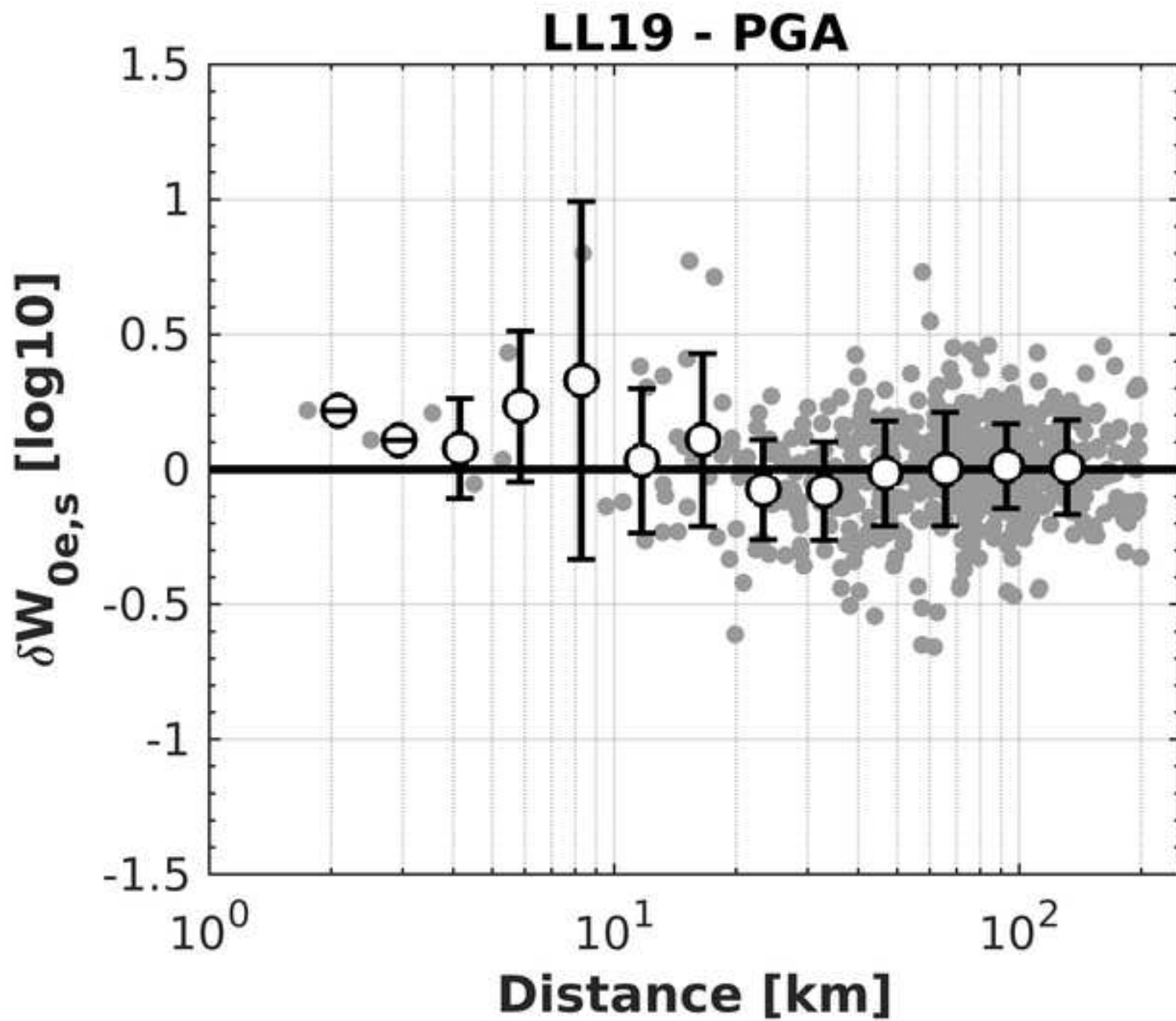












reply to reviewer's

[Click here to view linked References](#)



Click here to access/download
attachment to manuscript
review_2.docx



[Click here to view linked References](#)



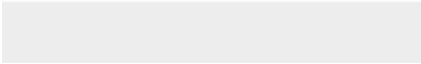

Click here to access/download
attachment to manuscript
s_mu.mat



[Click here to view linked References](#)




Click here to access/download
attachment to manuscript
esupp1_mod.csv



[Click here to view linked References](#)



Click here to access/download
attachment to manuscript
esupp3.pdf



[Click here to view linked References](#)



Click here to access/download
attachment to manuscript
read_me.txt



[Click here to view linked References](#)



Click here to access/download
attachment to manuscript
esupp2.pdf

